



DIPARTIMENTO DI FISICA

Corso di Laurea Triennale

Investigating the Bose-Hubbard model with IBM Quantum Experience

Supervisor:
Andrea Giachero

Co-Supervisor:
Stefano Barison

Candidate:
Pietro Campana

Id Number:
839735

ACADEMIC YEAR 2020/2021

Abstract

Quantum computers are a potentially powerful tool in the study of quantum many-body systems, achieving computations out of reach for their classical counterparts. Many purely quantum algorithms able to tackle physics problems with great accuracy have been proposed, but they still require resources beyond the limited hardware of current quantum computers. However, in recent years the development of a class of hybrid variational quantum-classical algorithms has already opened the possibility to employ this new technology in a variety of applications. This work focuses on the implementation of a Variational Quantum Eigensolver (VQE), finding the ground state of the two-site Bose-Hubbard model for different values of the boson interaction and low occupation numbers.

In the first chapter, the concept of quantum phase transitions is outlined, as well as giving a brief description of the second quantization formalism, which is used to write the Bose-Hubbard Hamiltonian. This model features a transition from a Mott insulator to a superfluid, caused by the interplay between competing terms of the Hamiltonian at different intensities, which is explained qualitatively. After describing some of the approaches used to compute its phase diagram, the discussion focuses on which quantum computational methods could be used to study or simulate this many-body system. An analysis of the simple two-site model follows, identifying two quantities, the entanglement entropy and the coherence visibility, which can be considered as a metric of the quantum correlations of the system, and will be used as reference values to be replicated by the quantum algorithm.

The second chapter features an introduction to quantum computation and to the tools that will be employed in the implementation of a VQE. After detailing qubits, gates and circuits, it presents the description of the services offered by IBM Quantum cloud platform, focusing on Qiskit and the systems, both hardware and simulators, accessible by its users, then outlining their properties, limitations and possible error mitigation methods. The basic structure of a Variational Quantum Algorithm is explained, followed by the description of some of the ansatze and classical optimizers that are commonly used in VQE instances, one of the possible applications of these kinds of algorithms.

The third chapter details the process of studying the two-site model by means of a VQE instance, starting from how to represent a system of bosons in a set of qubits and the choice of the ansatz. At first, different encodings and ansatze are tested in ideal

simulations of systems with two, three or four bosons, proving that they can perfectly replicate the result of the known solutions. Then, simulations featuring a realistic noise model show how much the current limits of quantum hardware can affect even relatively simple computations, such as these, requiring the introduction of error mitigation and post processing methods to partially recreate the system's correlation properties. Even so, the computed values remain largely dominated by systematic errors. For three bosons, a compact mapping and a simple ansatz that enforces the symmetry between sites obtain significantly better performances than the other tested combinations. This VQE instance is run on a real quantum computer, achieving qualitative correspondence with the values obtained by exact diagonalization. Considering numerical accuracy as a less than 5% deviation from the reference values with respect to the total excursion of the entanglement entropy, a quarter of the computed data satisfies this criterion. The results are commented in the concluding remarks, outlining a possible near-term extension of this approach to the simulation of systems with more sites.

Contents

Abstract	iii
Contents	v
List of Figures	vii
Introduction	1
1 The Bose-Hubbard model	5
1.1 Preliminary theoretical concepts	5
1.1.1 Quantum phase transitions	5
1.1.2 Second quantization	6
1.2 The model	8
1.2.1 Hamiltonian	8
1.2.2 Superfluid phase, negligible interactions	9
1.2.3 Mott insulator, null hopping	10
1.2.4 Phase diagram	10
1.2.5 Computing the phase boundary	11
1.2.6 Bose-Hubbard and quantum computation	12
1.2.7 Identifying the critical point	13
1.3 The two-site model	14
1.3.1 Hamiltonian and limit cases	14
1.3.2 Coherence visibility and entanglement entropy	16
2 Introduction to quantum computation	19
2.1 Basic concepts	19
2.1.1 Qubits	19
2.1.2 Circuits and computation	20
2.1.3 Single qubit gates	21
2.1.4 Multiple qubit gates	22
2.1.5 Gate decomposition and circuit transpiling	23
2.2 IBM Quantum cloud	24
2.2.1 Quantum Experience and Qiskit	24
2.2.2 Quantum Systems	24
2.3 Errors and decoherence	26

2.3.1	Limits of quantum hardware	26
2.3.2	Visualizing decoherence	27
2.3.3	Error correction	28
2.3.4	Error mitigation	28
2.4	The VQE algorithm	29
2.4.1	Variational quantum algorithms and the cost function	29
2.4.2	The ansatz	30
2.4.3	Optimizers	31
2.4.4	VQE and Qiskit	32
3	VQE and the two-site model	33
3.1	Mapping the problem	33
3.1.1	Bosons to qubits	33
3.1.2	Unary encoding	34
3.1.3	Gray encoding, N=3	35
3.2	Ansatze	36
3.3	VQE simulations and measurements	38
3.3.1	Statevector simulations	38
3.3.2	Unary coding, simulations with noise	40
3.3.3	N=3, Unary vs. Gray	43
3.3.4	Quantum hardware measurements	46
Conclusion		49
Bibliography		53

List of Figures

1	Matter wave interference patterns in the experimental realization of the Bose-Hubbard model[1], starting from a highly coherent state (a) that is progressively lost when intensifying the lattice potential (b-h).	2
1.1	The Bose-Hubbard model phase diagram computed for (a) three dimensional lattice, mean field approximation and (b) a two dimensional lattice, quantum Monte Carlo simulation[18].	11
1.2	Exact values of the entanglement entropy (a) and coherence visibility (b) for small numbers of bosons.	17
2.1	Bloch sphere representation.	20
2.2	A generic single-qubit quantum circuit.	20
2.3	A simple circuit generating the maximally entangled Bell state using one Hadamard and one <i>CNOT</i> gate.	23
2.4	Decomposition of a controlled- R_y with <i>CNOT</i> and single qubit rotation gates.	23
2.5	Properties of <i>ibmq_santiago</i> quantum computer.	25
2.6	Topological diagram of <i>ibmq_santiago</i>	26
2.7	Effect of relaxation from $ 1\rangle$ to $ 0\rangle$ in the Bloch sphere representation. .	28
2.8	Example of TwoLocal ansatz with two repetitions, linear connections and R_y rotations over three qubits.	31
3.1	Unary ansatz for $N = 2$	36
3.2	Unary ansatz for $N = 4$	37
3.3	Symmetrized unary ansatz for $N = 4$	37
3.4	Gray encoding, symmetric ansatz for $N = 3$	37
3.5	(a) $N = 3$ entanglement entropy values for the first statevector simulation, (b) energy residuals and difference between ground and first excited state energies.	38
3.6	(a) Statevector simulations with symmetric ansatze, (b) energy residuals. .	39
3.7	Noise reduction and correction applied to a noisy simulation for $N = 3$. .	40
3.8	Compared fidelities between standard and symmetrized unary ansatze. The table shows the fidelities means with standard deviations.	41
3.9	Computed visibility for noise model simulations with unary ansatze. .	42
3.10	Entanglement entropy values and residuals from noise model simulations of various occupation numbers with unary ansatz.	43
3.11	Fidelities for various ansatze, $N = 3$	44

3.12 Coherence visibility values and residuals from noise model simulations of $N = 3$ with best performing ansatze. The table shows the means and standard deviations of the residuals.	45
3.13 Best entanglement entropy values, residuals and relative error for the ground state energy, selected from two hardware runs using the symmetric Gray code ansatz for $N = 3$	46

Introduction

Some of the most exotic phenomena of Nature manifest when the effects of quantum mechanics are not overwhelmed by thermal fluctuations, with the emergence of peculiar properties such as superfluidity and superconductivity. Even at absolute-zero temperature, changing some parameter of a system may result in creating a phase transition which is driven by fluctuations that are only possible in quantum mechanics, in many cases determining the onset of collective behavior which propagates to a macroscopical scale. A paradigmatic quantum many-body system is the Bose-Hubbard model, describing interacting spinless bosons in a lattice, whose rich properties are exemplified in the Mott insulator to superfluid quantum transition. This model has been experimentally realized with ultracold ^{87}Rb atoms trapped in an optical lattice created by a laser[1]. Changing the intensity of the laser, the phase transition was induced, providing a way to destroy and restore at will long-range phase coherence in matter (Fig. 1). A possible important application that could arise from such a feat is the realization of interferometers with precision bound only by the Heisenberg uncertainty principle[2]. The Bose-Hubbard model is also employed in the study of granular superconductors, arrays of Josephsons junctions, and was even used as a toy model for the emergence of spacetime in a quantum gravity theory[3]. Being able to fully address the complexity of these systems could provide the key to invaluable theoretical insights and applications, but at the moment exactly simulating quantum many-body phenomena is incredibly difficult, even with the current powerful computational tools. The limit of computation does not reside much in the possibility of executing any problem, but doing so with limited resources of time and energy. Many tasks require computation times that scale exponentially with the dimension of the input, quickly becoming practically intractable. A quantum system, with its Hilbert space increasing exponentially in size with the number of basic objects involved, is naturally prone to provide a formidable challenge for classical computers. This is where the idea of quantum computation comes in place, stemming from the intuitions and pioneering works of Benioff, Feynman and Deutsch[4]: since Nature, at the best of our knowledge, is ultimately quantum mechanical, a controllable machine being able to embody its computational paradigm should be at least as powerful, if not more, than a classical computer. The field started to attract progressively more interest with the proposal of the first algorithms theoretically able to offer a computational speed up. One of the most famous is Shor's algorithm[5], able to factor integers exponentially faster.

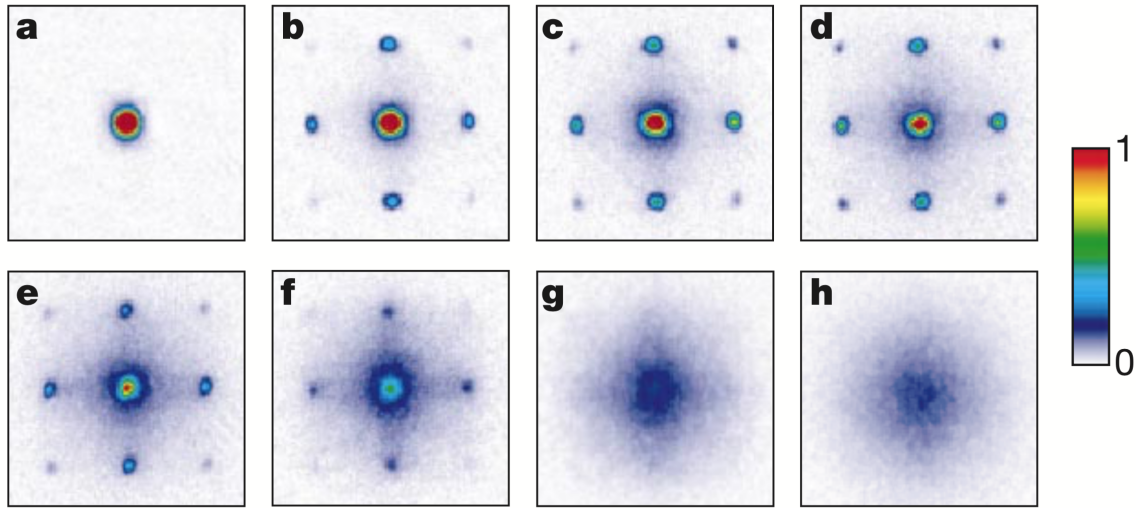


Figure 1: Matter wave interference patterns in the experimental realization of the Bose-Hubbard model[1], starting from a highly coherent state (a) that is progressively lost when intensifying the lattice potential (b-h).

The requirements for the physical implementation of a quantum computer were formalized by DiVincenzo[6], and the first experimental demonstration of an algorithm was realized at the end of the millennium[7]. From then, major advances have been made in the implementation of these machines, pursuing different physical realizations, most notably employing superconducting circuits, trapped ions and linear optics. The Bose-Hubbard model itself has been proposed as a platform for universal quantum computation[8], and can also describe superconducting qubits (the basic units of quantum information), since the Josephson junction is the principal component in their realization. As of now, demonstrating that it is possible to solve efficiently a problem infeasible by classical computation may have been already achieved in two instances, even if there have been some controversies. In 2019, Google announced that its superconducting quantum computer Sycamore completed in 200 seconds a task that would have required 10000 years employing the most powerful classical supercomputer at the time[9]. IBM, which owned it, disputed the claim affirming that with optimization the problem would only have required around two days to be solved. In the second case, by employing a photonic quantum computer implementing a boson sampling problem, researches from the University of Science and Technology of China claimed in december 2020 to have achieved a sample rate 10^{14} times higher than what would be possible with classical computation[10]. However, photonic computers of this scale are still not programmable and thus limited to execute specific tasks. Even if these are important milestones, saying that consistently achieving significant speed up in problems of practical interest will be possible is still an optimistic prediction. Moreover, we are living in what is called the Noisy Intermediate Scale Quantum (NISQ)[11] era of quantum computation, with devices that can already feature almost a hundred qubits, but are plagued by high error rates and still not easily scalable, making it impossible to implement error correction protocols.

Before the advent of fault tolerant quantum computation, it is still important to fully explore the capabilities of actual hardware. Some algorithms have been specifically designed to work in the NISQ era, one of them being the Variational Quantum Eigensolver, devised by Peruzzo et al. in 2014 [12], where a parametrized circuit on a quantum computer is iteratively optimized by classical means, trying to find the ground state of a system. In this hybrid scheme, the quantum computer just needs to prepare the state encoded by the circuit, which is one of the tasks that can fully exploit its peculiar capabilities. This work will be devoted to show the process and concepts involved when testing the VQE in a basic study of many-body systems, dealing with a simple instance of the Bose-Hubbard model.

Chapter 1

The Bose-Hubbard model

This chapter serves as an introduction to the rich many-body properties that are featured in this model and how they can be addressed both by classical and quantum computation, identifying in the two-site model a way to test the capabilities of a quantum algorithm.

1.1 Preliminary theoretical concepts

1.1.1 Quantum phase transitions

Many physical systems feature hamiltonians dependent on some parameters that change continuously for different configurations, for example regulating the interplay between the kinetic energy and some potential. For simplicity, let's consider one parameter g . Usually, one expects the energy of the ground state E_0 to be an analytic function of its values. However, in some special systems the first two energy levels cross at a certain critical point g_c . As a consequence, $E_0(g_c)$ is non-analytic. At $T = 0$, when the system is always in the ground state, the critical point is the boundary between two qualitatively different phases, with one of them featuring a different degree of order than the other, which can be quantified by a non-zero and non-unique order parameter that vanishes at the transition point. True level crossings are hard to achieve, and more commonly the non-analyticity results from the energy gap closing and progressively becoming more sharp when approaching the thermodynamic limit. In either cases, these systems undergo what is called a quantum phase transition[13], which is driven purely by quantum fluctuations instead of thermal ones. These phenomena are classified in various categories, one of the most important being known as second order, or continuous transitions, which feature some common properties.

Correlation length and energy scale

The order parameter fluctuates in all of the phases, even if its expectation value is zero in one of them. When approaching the critical point, the spatial correlations between its fluctuations become long ranged. More precisely, in second order transitions their

length scale ξ , called correlation length, diverges as:

$$\xi \propto |g - g_c|^{-\nu} \quad (1.1)$$

Where ν is known as the critical exponent. At the same time, the typical energy scale Δ at which there is a qualitative change in the frequency spectrum, which is simply the energy difference between the first two levels if the excitation spectrum is not gapless, vanishes as:

$$\Delta \propto |g - g_c|^{z\nu} \quad (1.2)$$

where z is called the dynamical critical exponent.

Universality

Apart from the correlation length and energy scale, there exist various other quantities that diverge or vanish with a power law governed by some exponent. A remarkable aspect of phase transitions is that these exponents are the same for very different microscopic realizations of the system, or even for apparently unrelated physical phenomena. Systems presenting the same behaviour near the critical point are said to belong to a specific universality class and have the same critical exponents.

Symmetry breaking

Many times, one of the two phases will not be invariant under a symmetry that instead is featured in the hamiltonian and in the other one. Thus, the symmetry is spontaneously broken when crossing the critical point going into the former phase, which is the one featuring a non-zero order parameter. The order parameter can be seen as an additional variable that becomes necessary to fully define the state when the symmetry is broken, but it is always present, even in non-symmetry breaking transitions.

1.1.2 Second quantization

When dealing with systems of indistinguishable particles, the wave function must be properly symmetrized or anti-symmetrized. Given a collection of N particle described by the states $|\psi_{\alpha_1}\rangle, |\psi_{\alpha_2}\rangle \dots |\psi_{\alpha_N}\rangle$, the collective state cannot be obtained naively composing them by tensor product. Neglecting normalization, it should be written as:

$$|\alpha_1, \alpha_2 \dots \alpha_N\rangle = \sum_P \zeta(P) |\psi_{P(\alpha_1)}\rangle \otimes |\psi_{P(\alpha_2)}\rangle \otimes \dots \otimes |\psi_{P(\alpha_N)}\rangle \quad (1.3)$$

Where P is one of the $N!$ possible permutations between the indices α_i defining the states, and $\zeta(P)$ is the parity of the permutation for fermions. For bosons, different α_i could still refer to the same state and $\zeta(P)$ is always 1. As can be seen, the typical wavefunction notation is not suited for the description of many body systems, especially when the total number of particle is not fixed, since it requires to compute a Slater determinant in case of fermions or a permanent for bosons any time it changes. Moreover, the total information about the system is still completely determined by the single particle wavefunctions. The second quantization formalism[14] aims to describe

the overall state only in terms of the number of particles n_i occupying each single particle one, which is limited to zero or one for fermions but can be any number for bosons. Noting that $\sum n_i = N$, this normalized state can be written as:

$$|n_0, n_1, n_2 \dots\rangle = \frac{1}{\sqrt{N! \prod_i n_i!}} |\alpha_1, \alpha_2 \dots \alpha_N\rangle \quad (1.4)$$

and is an element of the hilbert space \mathcal{H}_N . As can be seen, the number of particles in each state is well defined and, in the occupancy number notation, this is called a Fock state. Since both the occupations and the total number of particles can change, all of the possible Fock states can be seen as a basis for the Fock space, given by the direct sum of all \mathcal{H}_N :

$$\mathcal{F} = \bigoplus_{N=0}^{\infty} \mathcal{H}_N$$

The most important operators acting on this space are called the creation and annihilation operators, adding or subtracting one particle from the state they target. For bosons, they are defined as:

$$b_i^\dagger |n_0, n_1 \dots, n_i \dots\rangle = \sqrt{n_i + 1} |n_0, n_1 \dots, n_i + 1 \dots\rangle \quad (1.5)$$

$$b_i |n_0, n_1 \dots, n_i \dots\rangle = \sqrt{n_i} |n_0, n_1 \dots, n_i - 1 \dots\rangle \quad (1.6)$$

Any Fock state can be generated from the vaccum state $|0\rangle$ by applying b^\dagger :

$$|n_0, n_1 \dots, n_i \dots\rangle = \prod \frac{(b_j^\dagger)^{n_j}}{\sqrt{n_j!}} |0\rangle \quad (1.7)$$

and their commutation relations are a direct consequence of the spin-statistics theorem, generating their algebra:

$$[b_i, b_j] = [b_i^\dagger, b_j^\dagger] = 0, \quad [b_i, b_j^\dagger] = \delta_{ij} \quad (1.8)$$

$$\{c_i, c_j\} = \{c_i^\dagger, c_j^\dagger\} = 0, \quad \{c_i, c_j^\dagger\} = \delta_{ij} \quad (1.9)$$

where c_i are the fermionic operators. Another important operator is the one that counts the number of particles in a state:

$$\hat{n}_i = b_i^\dagger b_i, \quad \hat{n}_i |n_0, n_1 \dots, n_i \dots\rangle = n_i |n_0, n_1 \dots, n_i \dots\rangle \quad (1.10)$$

Finally, it can be shown that any operator can be written in terms of the creation and annihilation ones. Moreover, the second quantization formalism makes it possible to write efficiently many-body operators, proving to be superior to the first quantization language also in the description of interactions.

Coherent states

Even if not hermitian, it is still possible to write the eigenstates of the annihilation operator as a combination of different Fock states. These special wavefunctions are called coherent states, which in the first quantization can be seen as gaussian wave packets minimizing the uncertainty relation between momentum and position. More generally, if β is the complex-valued eigenvalue of a bosonic annihilation operator:

$$b|\beta\rangle = \beta|\beta\rangle \quad \beta = |\beta|e^{i\phi} \quad (1.11)$$

then the coherent state $|\beta\rangle$ can be written as:

$$|\beta\rangle = e^{-\frac{|\beta|^2}{2}} \sum_{n=0}^{\infty} \frac{\beta^n}{\sqrt{n}} |n\rangle = e^{-\frac{|\beta|^2}{2}} e^{\beta b^\dagger} |0\rangle \quad (1.12)$$

Another important property of the coherent state is that the total number of particles features a poissonian distribution characterized by mean and variance both equal to $|\beta|^2 = (\Delta n)^2 = \langle n \rangle$. Furthermore, the uncertainties of phase and number are related, obtaining $\Delta\phi\Delta n = 1/2$ in the limit $|\beta| \gg 1$, even though this is not a real uncertainty relation: similarly to time, the "phase" operator cannot be defined in quantum mechanics.

1.2 The model

1.2.1 Hamiltonian

The second quantization hamiltonian of the Bose-Hubbard model reads:

$$\hat{H} = -J \sum_{\langle i,j \rangle} b_i^\dagger b_j + \frac{U}{2} \sum_i \hat{n}_i(\hat{n}_i - 1) - \mu \sum_i \hat{n}_i \quad (1.13)$$

where $\langle i,j \rangle$ refers to first-neighbor lattice sites. The model can be obtained from the many-body hamiltonian for a gas of interacting spinless bosons under the following restrictions:

- The gas is sufficiently diluted, and only two-body interactions are considered.
- For short ranged potentials and near-zero temperature, the two-body interactions can be reduced to contact s-wave scattering.
- Due to the lattice, the field operators are expanded in the tight binding lowest band approximation.

As can be seen, the interplay between three different parameters will define the phase space of the system, the first one being the hopping term J , which quantifies the tunnelling between sites given by the kinetic energy of the particles and the single site trapping potential. The second one is the interaction term $\frac{U}{2} \sum_i \hat{n}_i(\hat{n}_i - 1)$, whose expression can be seen as a direct consequence of the contact potential, counting the

possible $\frac{1}{2}n_i(n_i - 1)$ pairs between n_i bosons in a site. Finally, the chemical potential μ regulates the total number of particles in the system. The ground state is usually studied for different values of J/U and μ/U . A homogeneous lattice at $T = 0$ with m sites is considered, excluding a global confining potential that could be introduced generalizing μ to a site-specific energy offset ε_i .

1.2.2 Superfluid phase, negligible interactions

Generally, since bosons do not need to satisfy the Pauli exclusion principle, a macroscopic portion of the particles can condense into a single state when the temperature is sufficiently low, forming a Bose-Einstein condensate, a state of matter which is deeply connected with superfluidity. For negligible interactions $U \ll J$, the hamiltonian is easily diagonalizable by a Fourier transform. Free to hop between the sites of the lattice, at $T = 0$ all of the particles condense into the zero momentum state. For a fixed number of particles N the ground state is well approximated by:

$$|SF(N)\rangle = \left(\frac{1}{\sqrt{m}} \sum_{i=0}^m b_i^\dagger \right)^N |0\rangle \quad (1.14)$$

and all the bosons occupy the same extended Bloch state, or atomic coherent state[15]. In the grand canonical ensemble, fixed the average density $\langle \hat{n}_i \rangle = N/m = n$, the ground state can be written as a product of onsite coherent states:

$$|SF(n)\rangle = \prod_{i=0}^m |\beta_i = \sqrt{n}\rangle \propto \prod_{i=0}^m \left(e^{\sqrt{n}b_i^\dagger} \right) |0\rangle \quad (1.15)$$

Either way, the ground state is described by macroscopic wave functions with long-range coherence over the lattice, which become very similar in the thermodynamic limit. The particles are completely delocalized and their distribution in every site is poissonian. This kind of system can be described as a weakly interacting bose gas, which is extensively studied in the literature. In particular, the Bogoliubov theory[16] shows that its excitation spectrum is gapless and satisfies Laundau's criteria for superfluidity. A very important feature of the ground state is its great degeneracy, since it has the same energy for any possible phase that could be added to \sqrt{n} . This causes the spontaneous breaking of the $U(1)$ gauge symmetry of the hamiltonian, which always conserves the total number of bosons and is thus invariant under the transformation:

$$V_\phi = \exp \left(i\phi \sum_j \hat{n}_j \right) \quad (1.16)$$

Since the ground state is an eigenvector of the boson annihilation operator, which instead changes under the transformation, it is not invariant and a phase ϕ is added to its expectation value, which can be considered as the order parameter of the transition. This must be done with caution, since some superpositions of coherent states will be a valid ground state but feature overall null expectation value. Symmetry breaking can still be detected considering the degeneracy, or by defining a different order parameter.

1.2.3 Mott insulator, null hopping

Considering the limit case $J = 0$, an integer number n of bosons is perfectly localized in each site, where $n - 1 < \mu/U < n$. The ground state is simply the product between the m local Fock states:

$$|MI\rangle \propto \prod_{i=0}^m (b_i^\dagger)^n |0\rangle \quad (1.17)$$

and the system is in what is called the Mott insulator phase, featuring perfect correlation between each site's particle number and no phase coherence, with null order parameter. This phase is also characterized by null compressibility $\frac{\partial n}{\partial \mu}$ and a finite energy gap between the first excitation and the ground state, given by adding a particle to the system when μ/U is closer to n or subtracting one, creating a hole, for μ/U closer to $n - 1$. If the total number of particles is to be conserved, the first excitation is a sum of these two and requires an energy U . An interesting case is given by μ/U being exactly n , where there is no difference between having $n + 1$ bosons or n per site, so the particles are free to hop around the lattice, bose condensing and generating a superfluid phase even at $J = 0$ for this ideal system.

1.2.4 Phase diagram

The first important consideration when trying to describe the phase diagram of the Bose-Hubbard model is that any number of particles that can hop through the lattice without energy cost will condense in a superfluid, as in the extreme case $J=0$, $\mu/U=n$, integer n . When J is increased from zero, the energy necessary to create an excitation in the insulating phase decreases, since the created particle or hole gains a kinetic energy which increases with J . For a constant J , there are values of μ for which the energy cost vanishes and the onset of superfluidity takes place, defining the phase boundaries. For large enough values of J , this will be true for any μ and the boundaries will close, leaving only the superfluid phase. This qualitative description helps to understand the phase diagram in the plane J/U vs μ/U , characterized by Mott insulating lobes for every integer filling factor n (the same number of bosons in every site), surrounded by the superfluid (Fig. 1.1). When the total number of particles is conserved the density is fixed, and the phase transition can be observed only if N is commensurate with the number of sites. Since any other fixed-density line of the diagram skirts around the phase boundaries, remaining in the superfluid state, every integer filling factor one must cross perpendicularly the tip of the respective lobe, otherwise the superfluid would have a non physical negative compressibility in its proximity. If d is the dimensionality of the model, this special multi-critical point exhibits a transition belonging to the universality class of the XY classical model in $(d + 1)$ dimensions[17]. For example, the 2-D Bose-Hubbard model should present the same critical behaviour of the lambda transition of superfluid ${}^4\text{He}$ in 3-D nanoporous media. It should be noted that the transition in 1-D is different from the other cases, since it is of the Berezinskii-Kosterlitz-Thouless type, which is an infinite order transition characterized by exponential divergence of the correlation length and no symmetry breaking. It is then important to keep in mind that the methods used to simulate or compute the properties of this system in 1-D often cannot be straightforwardly extended to higher dimensions.

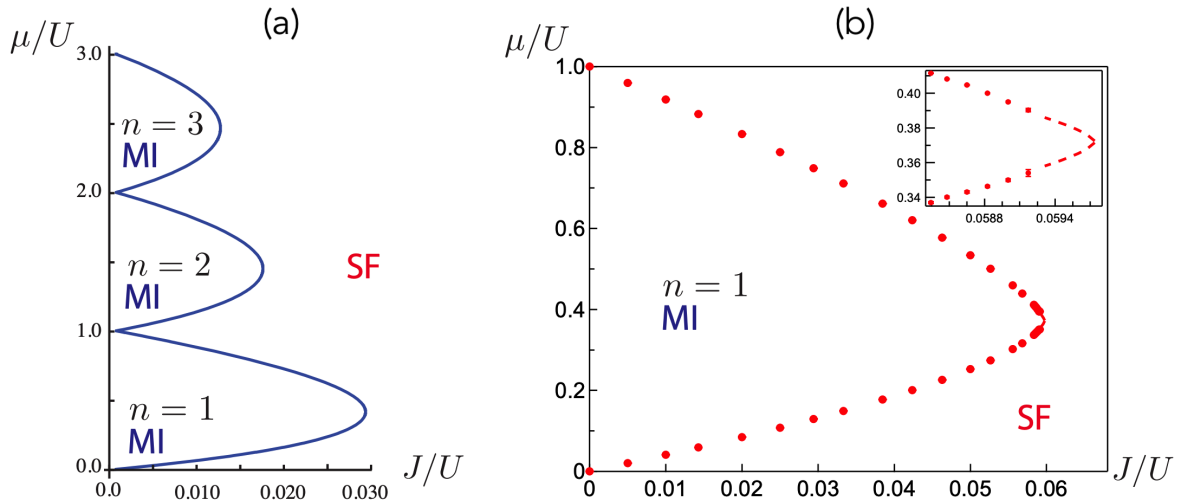


Figure 1.1: The Bose-Hubbard model phase diagram computed for (a) three dimensional lattice, mean field approximation and (b) a two dimensional lattice, quantum Monte Carlo simulation[18].

1.2.5 Computing the phase boundary

The first approach to the calculation of the phase boundary is given by the mean field approximation, decoupling the hamiltonian into m single-site terms. This approximation is fairly valid for the 2-D and 3-D model, giving an analytic expression of the boundary that presents the characteristic lobes. In reality, the lobes are sharper than the mean-field predictions and have a very different shape in the 1-D case. More precise calculations have been carried out using a variety of approaches, the most notable ones being;

- **Quantum Monte Carlo:** Since bosons do not present the sign problem[19], almost exact computations can be carried out using quantum Monte Carlo simulations, in various cases employing the Worm algorithm [18][20]. Even if providing the most precise results, which are used as reference values for the experimental realizations of the system, large scale Quantum Monte Carlo simulations require great computational resources and are usually limited to very low or unitary filling factors and small lattices (Fig. 1.1).
- **Strong coupling expansion:** An analytic calculation of the diagram can be obtained starting from the Mott phase and employing a perturbative expansion with respect to the kinetic energy[21]. This method provides accurate estimates for low J , but deviates from the Monte Carlo results when approaching the tip of the lobes. However, it is still useful, since it can be applied for arbitrary integer filling factors.
- **Density matrix renormalization group (DMRG):** Another quasi-exact numerical method is provided by systematically truncating the Hilbert space while the dimension of the system is progressively increased, keeping the most useful

wave functions[22]. This is one of the most profitable algorithms for the study of 1-D lattice systems, but similarly to Monte Carlo, for the Bose Hubbard model very precise calculations can be carried out only for low filling numbers.

1.2.6 Bose-Hubbard and quantum computation

Even when limiting the number of bosons that can occupy a site, the Hilbert space that must be considered for an exact simulation of the Bose-Hubbard model still grows exponentially with the number of sites, quickly becoming intractable with classical computation. Current methods already achieve a great degree of accuracy, but quantum computation could provide full control of the Hilbert space and create exact simulations with a number of qubits that essentially grows only as the number of bosons involved, since the space spanned by N qubits is 2^N dimensional. If quantum computers will become more scalable and reliable, a general simulation algorithm that is easily adaptable to various dimensionalities or filling factors and at the same time more precise than Quantum Monte Carlo could be implemented. At the moment this is still nothing more than a prediction, but many algorithms that could be used to study complex systems have already been proposed.

Quantum digital simulation

It is the direct simulation of time evolution of an initial state under a hamiltonian. On a quantum computer, this consists of creating a circuit that approximates the exponentiation of the hamiltonian for small time-steps, measuring the energy expectation value at different times and recovering the energy spectra of the state's evolution by applying a Fourier transform. Alternatively, the eigenvalues of any unitary operator can be recovered with the Quantum Phase Estimation algorithm[23]. Generally, the hamiltonian will feature different non-commuting terms, for example $H = A + B$, $[A, B] \neq 0$, but for a small enough time step the first order Trotter approximation:

$$e^{i(A+B)\Delta t} \approx e^{iA\Delta t} e^{iB\Delta t} \quad (1.18)$$

permits to exponentiate the terms in a straightforward way. Even if this algorithm was successfully run on a simulation of a quantum computer for a small Bose-Hubbard system[24], it is still far out of reach for current NISQ hardware, requiring very complex circuits.

Analog simulation

Remarkably, the hard-core Bose-Hubbard model, with each site occupied only by one or zero bosons, is naturally realized by an array of Josephson junctions, the basic components of the transmon qubit[25]. Blending experimental realization and computation, quantum computers based on this technology might physically simulate the system while potentially having control over the single sites. However, the simulation is possible only for parameters that are in the Josephson junction's working regime. In this case their negative anharmonicity corresponds to the weak attractive interaction regime of the Bose-Hubbard model, very different from the cases considered in this

brief description of the quantum phase transition. This possibility is still interesting, since the system exhibits the emergence of many-body properties in some regions of its energy spectrum.

Imaginary time evolution

Replacing the cumbersome time evolution with imaginary time drives the energy closer to its minimum value at each iteration, which could be used to find the ground state of various systems[26]. Since the imaginary time evolution operator is not unitary, while quantum computation requires unitarity, it must be approximated with a unitary transformation. However, this approximation must extend to the qubits that are correlated with the one that is targeted by a term of the imaginary time evolution operator. Since the correlation length diverges at the critical point, the phase transition becomes impossible to simulate exactly. This approach could still be used for regimes that feature limited correlations.

Variational Quantum Algorithms

The previously outlined approaches to the Bose Hubbard model with quantum computation clearly can address only some features of the system or require inconsiderate quantum resources. Using a variational algorithm, which will be described in detail in the next chapter, part of the computational cost is streamlined to a classical computer, making it possible to use this class of programs with current quantum hardware. Moreover, these kind of algorithms could be adapted to describe both of the phases of the model and the phase transition, since the variational ansatz can be chosen to encode arbitrary states in the qubits Hilbert space. Ideally, one of these algorithms could be used to compute the ground state of the model for any parameter of the hamiltonian, perfectly defining the phase boundaries. Obviously, its implementation cannot start by addressing the full complexity of the Bose-Hubbard model, but must first be restricted to some simpler aspects. Recently, two other works have studied the connection between this model and VQAs, the first one trying to replicate the ground state in the attractive interaction regime with a photonic quantum computer[27], the second one implementing a quantum machine learning algorithm for the detection of phase transitions[28].

1.2.7 Identifying the critical point

Let's start by considering only the special transitions at integer filling factors. Fixing the number of particles, the energy term dependent by the chemical potential is constant and can be neglected. It is important to define the quantities that can be used to detect the phase transition. Many observables and metrics have already been employed in the discussions of the model, some of them being the superfluid density, the compressibility, the order parameter, the energy gap and the correlation lenght, which can be extracted from various correlation functions. Between these, a very simple and easily accessible, both by experimental means and by a quantum computer, could be the nearest-neighbor correlation function[29].

Given $u = U/J$ and identifying the ground state with $|u\rangle$, this correlator can be written as:

$$C(u) = \langle u | b_i^\dagger b_j + b_j^\dagger b_i | u \rangle |_{\langle i,j \rangle} \quad (1.19)$$

In the thermodynamical limit, the critical point should manifest as a singularity of one of the derivatives of this function, the second in the case of a 2-D lattice and the first for three dimensions. For finite systems, the derivatives of $C(u)$ will become smooth, but will still present a peak around the critical point. It must be noted that, since the correlation length in the 1-D model diverges exponentially, this method cannot be applied. To set the range of parameters that must be covered when simulating or studying the transition, it would be useful to know in advance where it takes place. Fortunately, an empirical expression has been found[30] that can well approximate the position of the critical point both for any integer filling factor n and realistic dimensionality D :

$$\left(\frac{U}{DnJ} \right)_{crit} = a + bn^{-c} \quad (1.20)$$

Where the parameters a, b, c are shown in Table 1.1.

D	a	b	c
1	2.16	0.97	2.13
2	5.80	2.66	2.19
3	6.70	3.08	2.18

Table 1.1: Parameters of the empirical expression approximating the critical point for different dimensionalities D .

1.3 The two-site model

1.3.1 Hamiltonian and limit cases

The simplest system featuring a Bose-Hubbard hamiltonian consists of a few bosons trapped in a symmetric double-well potential. It provides a way to benchmark and study core aspects of many-body properties and phase transitions even with limited NISQ hardware, offering viable analytic expressions for the problem's eigenvectors and quantities regarding quantum correlations[31]. For a fixed number N of bosons, there exist $N+1$ orthogonal occupation states which can be written as the Fock basis $|i, N-i\rangle = |i\rangle_L \otimes |N-i\rangle_R$, where i is the number of bosons in the left well. The hamiltonian:

$$\hat{H} = -J(b_R^\dagger b_L + b_L^\dagger b_R) + \frac{U}{2}[\hat{n}_R(\hat{n}_R - 1) + \hat{n}_L(\hat{n}_L - 1)] \quad (1.21)$$

can be represented as a $(N+1) \times (N+1)$ matrix in the Fock basis and is easily diagonalizable for small numbers of bosons. Being interested in phase transitions for $T = 0$, the following considerations will focus on the properties of the ground state for

different values of the parameters U and $J > 0$. Let's start by considering the three possible limit cases, all showing really different characteristics:

- $U = 0$: in the absence of interaction, given $|0, 0\rangle$ the vacuum state of the Fock space, the ground state is the atomic coherent one:

$$\frac{1}{\sqrt{N!2^N}} \left(b_L^\dagger + b_R^\dagger \right)^N |0, 0\rangle \quad (1.22)$$

presenting analogies with the superfluid phase of the larger systems. The probability distribution of the possible occupations ordered for increasing i is approximately gaussian.

- $J \rightarrow 0, U < 0$: even if for strong enough attractive interactions the collapse of the system will take place, in this limit the ground state tends to a macroscopic superposition of the two opposite occupations:

$$\frac{1}{\sqrt{2}} (|N, 0\rangle + |0, N\rangle) \quad (1.23)$$

This kind of superposition is commonly referred to as the Schrödinger cat state, while in this case it is also known as the *NOON* state. It is very delicate, since the energy difference between the ground and the first excited state quickly tends to zero for stronger attractions[32].

- $J \rightarrow 0, U > 0$: Strong repulsions localize the particles in their respective wells. Even with this simplified system, a notable difference arises in this regime between instances where N is even (integer filling factor) or N is odd, thus not commensurate with the number of sites. In the first case, the increasing interaction brings the system from the simil-coherent state to the fully incoherent twin Fock state:

$$\left| \frac{N}{2}, \frac{N}{2} \right\rangle \quad (1.24)$$

while, in the latter case, the symmetry between sites $\langle \hat{n}_L \rangle = \langle \hat{n}_R \rangle$ keeps the system partially entangled, and the ground state tends to the superposition:

$$\frac{1}{\sqrt{2}} \left(\left| \frac{N+1}{2}, \frac{N-1}{2} \right\rangle + \left| \frac{N-1}{2}, \frac{N+1}{2} \right\rangle \right) \quad (1.25)$$

making it impossible to fully localize the particles.

It can already be seen how the interplay between the parameters changes the nature of the ground state similarly to the bigger system. Since the hamiltonian can still easily be diagonalized for low occupation numbers, the exact ground state can be found and expressed in terms of superposition of the possible occupations $|i, N-i\rangle$ with respective amplitudes c_i . From now on, J is normalized to 1, and the amplitudes

have an analytic expression in $U/J = U$. As an example, for $N=3$ the ground state is:

$$|E_G\rangle = A_3 \left[|0,3\rangle + |3,0\rangle + \frac{1+U+\sqrt{4+2U+U^2}}{\sqrt{3}}(|1,2\rangle + |2,1\rangle) \right] \quad (1.26)$$

$$A_3 = \left[2 + \frac{2}{3}(1+U+\sqrt{4+2U+U^2})^2 \right]^{-\frac{1}{2}} \quad (1.27)$$

1.3.2 Coherence visibility and entanglement entropy

After giving a qualitative description of the possible states of the model, it is useful to introduce some parameters to evaluate the extent of the correlations in the system. These quantities should also be easily accessible by the quantum algorithm one wants to develop in order to compare its performance with the standard solutions. The first one is given by the expectation value of the hopping term:

$$\alpha = \frac{2}{N} |\langle b_R^\dagger b_L \rangle| \quad (1.28)$$

Other than being really similar to the nearest-neighbor correlation function whose singularities detect the transition point, in the two site model this real quantity represents the visibility of the interference fringes of the momentum distribution:

$$n(\mathbf{p}) = 2n_0(\mathbf{p}) \left(1 + \alpha \cos\left(\frac{\mathbf{p} \cdot \mathbf{d}}{\hbar}\right) \right) \quad (1.29)$$

experimentally accessible by scattering based measurements, giving a measure of the coherence of the system. Here \mathbf{d} is the distance between the two sites and $n_0(\mathbf{p})$ is the momentum distribution in single well as in the fully incoherent regime. The coherence visibility has an analytic expression in U for the values of N considered that can be computed from the occupations amplitudes as:

$$\alpha = \frac{2}{N} \sum_{i=0}^N c_i^* c_{i+1} \sqrt{(i+1)(N-i)} \quad (1.30)$$

and attains its maximum value for the atomic coherent state. Another interesting quantity, measuring of the degree of quantum entanglement in the context of bi-partition, is the entanglement entropy, which can also be used to locate the critical point[33]. It is defined as the Von Neumann entropy of the reduced density matrix of one of the two subsystems. If a pure state describing the system is separable, then the reduced density matrix of a subsystem is also a pure state and the entropy is zero, while it is positive otherwise. For the two sites model, given $\hat{\rho} = |E\rangle \langle E|$ the density matrix of the ground state:

$$\hat{\rho}_{L,R} = \text{Tr}_{R,L}(\hat{\rho}) \quad (1.31)$$

$$S = -\text{Tr}(\hat{\rho}_{L,R} \log_2 \hat{\rho}_{L,R}) = -\sum_{i=0}^N |c_i|^2 \log_2 |c_i|^2 \quad (1.32)$$

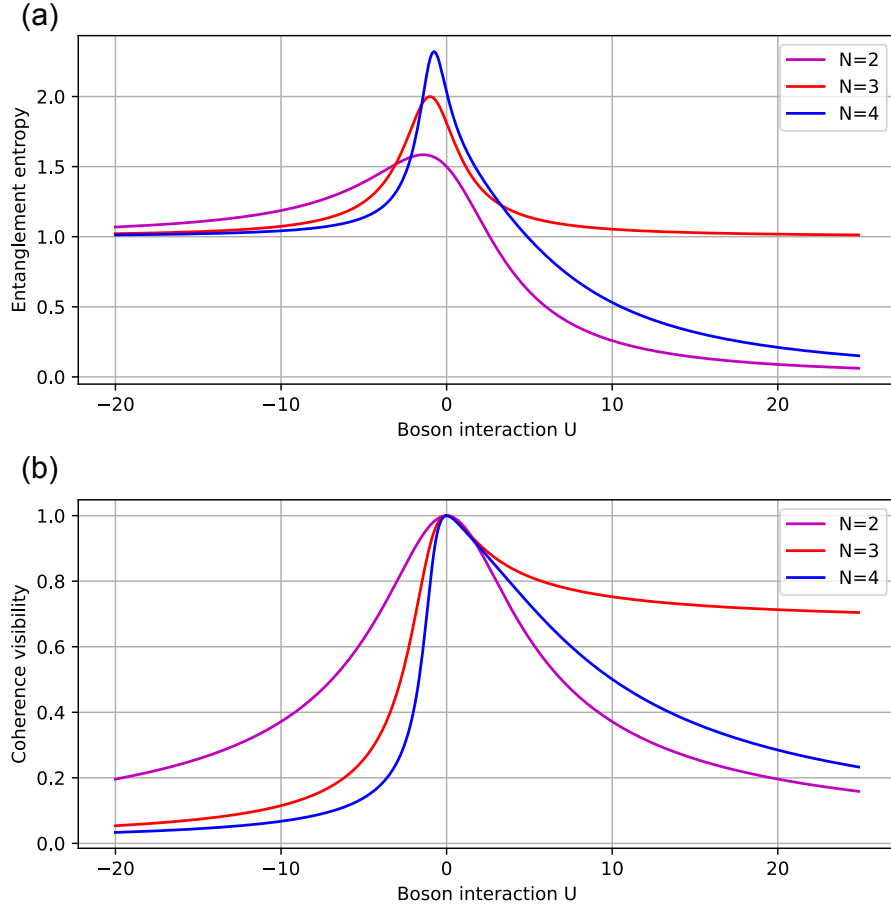


Figure 1.2: Exact values of the entanglement entropy (a) and coherence visibility (b) for small numbers of bosons.

The entanglement entropy is easily obtainable from the probabilities for the possible occupations, hence also having a viable analytic expression at least for low values of N . Because of this, it will be used together with the visibility as the principal target quantity that the quantum computation should be able to replicate, even if estimating the entropy for larger systems with a quantum algorithm is not as straightforward as measuring an observable[34]. Its extremant takes place for slightly attractive interactions, with a peak that becomes sharper and more pronounced for higher numbers of particles. Both the visibility and the entanglement entropy tend to zero for integer filling factors and great repulsive interactions, while they respectively reach $2/3$ and 1 in the same limit, but for odd N . Their exact values for the range $U \in [-20, 25]$ and $N = 2, 3, 4$ are plotted in Fig. 1.2. As can be seen, this range permits to appreciate almost all of the values that these established metrics can achieve, but might be too large to be covered by the lengthy simulations of a quantum algorithm. Even if in this case there is not a quantum phase transition and the system is very different from the one in the thermodynamic limit, Eq. 1.20 can still be employed to achieve some insight on the possible critical point, locating it at $U = 3.128$ for unitary filling factor and $U = 5.348$ for filling factor 2. Thus, a reasonable range from which to start when first employing the quantum algorithm could be $U \in [0, 10]$.

Chapter 2

Introduction to quantum computation

After identifying the physical system that will be addressed in this work, the core concepts and instruments of quantum computation are presented, focusing on circuits and gates, the IBM Quantum cloud platform, errors and the Variational Quantum Eigensolver algorithm.

2.1 Basic concepts

2.1.1 Qubits

Abstracting from its physical implementation, a qubit is a two levels quantum system, featuring an orthonormal basis given by:

$$|0\rangle = \begin{pmatrix} 1 \\ 0 \end{pmatrix}, |1\rangle = \begin{pmatrix} 0 \\ 1 \end{pmatrix},$$

carrying the basic unit of information, similarly to the two values encoded in a classical bit. However, for a qubit any unitary superposition of the computational basis vectors:

$$|\psi\rangle = \alpha|0\rangle + \beta|1\rangle, \quad |\alpha|^2 + |\beta|^2 = 1 \tag{2.1}$$

where $\alpha, \beta \in \mathbb{C}$, is also a legitimate state of the system. Even if admitting an infinite number of states, when a measurement in the computational basis is carried out the collapse takes place and either $|0\rangle$ or $|1\rangle$ is observed, with respective probabilities $|\alpha|^2$ or $|\beta|^2$. Since an overall phase never influences the outcome of a measurement, any meaningfully different state can be written as:

$$|\psi\rangle = \cos\left(\frac{\theta}{2}\right)|0\rangle + e^{i\phi}\sin\left(\frac{\theta}{2}\right)|1\rangle \tag{2.2}$$

where $\theta, \phi \in \mathbb{R}$ can be interpreted as the polar and azimuthal coordinates for a unitary sphere. Any single-qubit state is thus mapped to a point on its surface, and this representation is known as the *Bloch sphere* (Fig. 2.1).

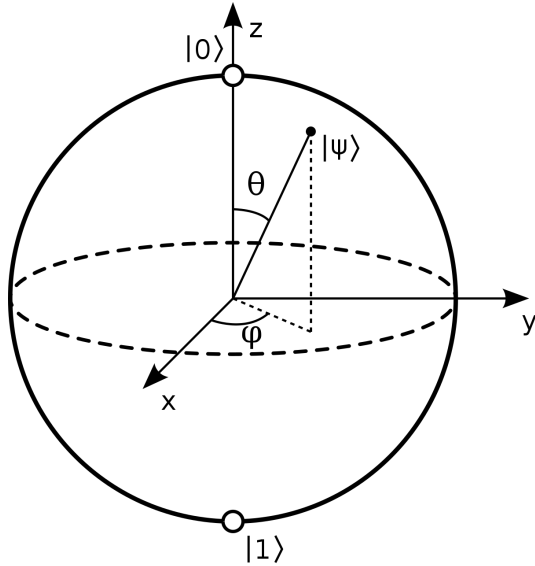


Figure 2.1: Bloch sphere representation.

The computational basis is aligned with the z axis of the sphere, while two other common basis $|+\rangle, |-\rangle$ and $|\circlearrowleft\rangle, |\circlearrowright\rangle$, to the x and y axis respectively.

$$|+\rangle = \frac{|0\rangle + |1\rangle}{\sqrt{2}} = \frac{1}{\sqrt{2}} \begin{pmatrix} 1 \\ 1 \end{pmatrix}, \quad |-\rangle = \frac{|0\rangle - |1\rangle}{\sqrt{2}} = \frac{1}{\sqrt{2}} \begin{pmatrix} 1 \\ -1 \end{pmatrix} \quad (2.3)$$

$$|\circlearrowleft\rangle = \frac{|0\rangle + i|1\rangle}{\sqrt{2}} = \frac{1}{\sqrt{2}} \begin{pmatrix} 1 \\ i \end{pmatrix}, \quad |\circlearrowright\rangle = \frac{|0\rangle - i|1\rangle}{\sqrt{2}} = \frac{1}{\sqrt{2}} \begin{pmatrix} 1 \\ -i \end{pmatrix} \quad (2.4)$$

2.1.2 Circuits and computation

Computation on a quantum computer can be seen as an operation producing an output state $|\psi'\rangle$ from the input $|\psi\rangle$. The norm of the state must be preserved, and if the output is definite the computation corresponds to a linear unitary transformation associated to an operator \hat{U} . As classical computation is carried out by applying logic gates to a set of bits, so in its quantum counterpart a program is encoded by a set of unitary operators, called quantum gates, acting on the qubits. This can be represented as a quantum circuit, where every qubit corresponds to a wire connecting the gates, acting from left to right. A special operation is the measurement, which collapses the state to one of the possible vectors of the basis over which the measurement is carried out, usually the computational one (Fig. 2.2). The outcome can then be saved on a classical bit, and information on the state is recovered from the outcomes' probabilities by repeating the computation many times.

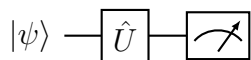


Figure 2.2: A generic single-qubit quantum circuit.

It is worth noting that, due to unitarity, until any qubit is measured all of the computation is reversible. However, many useful applications, such as preparing mixed states, or even entire quantum computation paradigms[35] are based on the strategic application of measurement, sacrificing reversibility. An important feature of a circuit is its depth, defined as the minimum number of distinct time steps required for its execution, roughly corresponding to the longest path between gates from the input to the output. Time complexity and depth are limited in near-term hardware, becoming both a measure of its possible performance and some of the main properties that must be addressed in the optimization of a circuit.

2.1.3 Single qubit gates

Any single-qubit operation can be expressed as a unitary 2×2 matrix. There are many common gates that serve as the building blocks of quantum computation, relevant both in its theory and in the physical implementations of quantum computers.

Pauli

Together with the identity $I = \sigma_0$, the Pauli matrices

$$\sigma_1 = X = \begin{pmatrix} 0 & 1 \\ 1 & 0 \end{pmatrix} \quad \sigma_2 = Y = \begin{pmatrix} 0 & -i \\ i & 0 \end{pmatrix} \quad \sigma_3 = Z = \begin{pmatrix} 1 & 0 \\ 0 & -1 \end{pmatrix}$$

Form a basis for the 2×2 matrices space, and act in fundamental ways on a qubit. For example, X serves as the quantum counterpart to the classical *NOT* operation, exchanging $|0\rangle$ and $|1\rangle$:

$$\alpha|0\rangle + \beta|1\rangle \quad \xrightarrow{\boxed{X}} \quad \alpha|1\rangle + \beta|0\rangle$$

While Z flips the phase of $|1\rangle$.

$$\alpha|0\rangle + \beta|1\rangle \quad \xrightarrow{\boxed{Z}} \quad \alpha|0\rangle - \beta|1\rangle$$

Hadamard

The hadamard gate:

$$H = \frac{1}{\sqrt{2}} \begin{pmatrix} 1 & 1 \\ 1 & -1 \end{pmatrix}$$

is used in many applications, since it switches from the computational basis to the $|+\rangle, |-\rangle$ one, creating an equal superposition of $|0\rangle$ and $|1\rangle$ when starting from one of them. If it is applied to every qubit in a set where every one of them is initialized in $|0\rangle$, it creates an equal superposition between all the possible numbers they can encode.

$$\alpha|0\rangle + \beta|1\rangle \quad \xrightarrow{\boxed{H}} \quad \alpha|+\rangle + \beta|-\rangle$$

Rotations

Since all the possible states form a continuum, it is useful to have some gates whose action can be finely tuned by a single or a set of parameters. This is the case of the rotation gates, obtained exponentiating the Pauli ones, for example:

$$R_x(\delta) = e^{i\delta X} = \cos(\delta)I - i \sin(\delta)X$$

The action of these gates is equivalent to a 2δ rotation around their respective axes in the Bloch sphere representation.

S and T gates

Also known as the roots of Z , these gates change the relative phase in the computational basis:

$$S = \sqrt{Z} = \begin{pmatrix} 1 & 0 \\ 0 & i \end{pmatrix} \quad T = \sqrt{S} = \begin{pmatrix} 1 & 0 \\ 0 & e^{\frac{i\pi}{4}} \end{pmatrix}$$

as in a quarter-turn or eight-turn around the z axis.

2.1.4 Multiple qubit gates

Applying the gates described until now to a set of qubits, the resulting state can always be written as a tensor product of the single qubit ones. However, it is known that entangled states do not satisfy this property. Entanglement is, together with superposition, one of the core concepts of quantum mechanics that is employed in quantum computation, making it possible to fully explore the 2^N Hilbert space spanned by N qubits.

CNOT

Entangling gates must act at least on two qubits, the most important being the *CNOT* (controlled-*NOT*) gate. Generally, a controlled gate applies its operation, in this case \oplus , only when the control qubit is in $|1\rangle$. With this operation, entangled states can be created even with a simple circuit, such as in Fig. 2.3, where the measurement of one of the qubits determines the outcome of the other. *CNOT* is represented as:

$$CNOT = \begin{pmatrix} 1 & 0 & 0 & 0 \\ 0 & 1 & 0 & 0 \\ 0 & 0 & 0 & 1 \\ 0 & 0 & 1 & 0 \end{pmatrix} \quad \text{Diagram: } \begin{array}{c} \text{---} \bullet \text{---} \\ | \qquad \oplus \\ \text{---} \text{---} \end{array}$$

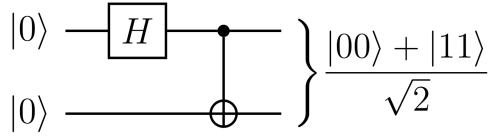


Figure 2.3: A simple circuit generating the maximally entangled Bell state using one Hadamard and one $CNOT$ gate.

SWAP

This gate swaps $|0\rangle$ and $|1\rangle$ between the qubits it connects:

$$SWAP = \begin{pmatrix} 1 & 0 & 0 & 0 \\ 0 & 0 & 1 & 0 \\ 0 & 1 & 0 & 0 \\ 0 & 0 & 0 & 1 \end{pmatrix} \quad \text{Diagram: } \begin{array}{c} * \\ - \\ - \\ * \end{array}$$

2.1.5 Gate decomposition and circuit transpiling

An important concept is that of universal gate set, a finite collection of gates that can implement all the possible operations in quantum computation[36]. Since the number of gates is uncountable, this cannot be done exactly, but it is still possible to approximate any operation with some finite sets. The standard set of universal gates consist of H , S , T and $CNOT$, which can not only approximate any circuit but also do it fault-tolerantly. Real universal quantum computers usually physically implement a set given by $CNOT$, a rotation and other single qubit gates. If gate decomposition consists of expressing a gate in terms of other, circuit transpiling is the process of optimally translating a circuit to the gates and connections available by the hardware. Typical examples of gate decomposition are the implementation of control on other standard gates, such as controlled-rotations, using $CNOT$ (Fig. 2.4), or the decomposition of $SWAP$ in three alternating $CNOT$. In near-term applications, it is important to check if transpiling a circuit to the gates implemented on a real device can be done without increasing its depth excessively.

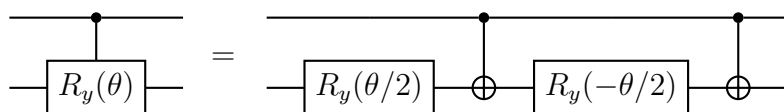


Figure 2.4: Decomposition of a controlled- R_y with $CNOT$ and single qubit rotation gates.

2.2 IBM Quantum cloud

2.2.1 Quantum Experience and Qiskit

Since 2016, IBM offers a variety of services regarding quantum computation under the collective name of IBM Quantum. Most of the programming work of this thesis has been done on what is commonly known as IBM Quantum Experience¹, a section of IBM's quantum cloud platform featuring the Quantum Composer, Lab and access to various hardware systems or simulators[37]. The Composer is a graphical interface aiding in the design and construction of quantum circuits, supporting both real time simulation of the results and hardware runs. The Quantum Lab is a virtual environment for the development of Jupyter notebooks or code featuring Qiskit, a Python-based open source software development kit. Qiskit is organized in modules, the main ones being:

- **Terra**: composition of quantum programs from the fundamental circuits and pulse control.
- **Aer**: noise models, circuits extensions and simulators.
- **Ignis (deprecated)**: characterization of errors and noise mitigation.
- **Aqua (deprecated)**: development and library of quantum algorithms.
- **Qiskit IBM Quantum provider**: backend provider and jobs manager.

As of today, Qiskit is refactoring Aqua in four modules dedicated to the different fields of application of quantum algorithms, such as Qiskit Nature for quantum chemistry and the natural sciences. In future releases, Ignis will also be refactored to Qiskit Experiments. The VQE used in this thesis has been developed using the four original "elements" modules due to the better stability of older Qiskit releases.

2.2.2 Quantum Systems

Hardware systems

Real universal quantum computers featuring up to five qubits are freely accessible with a basic account. These devices are all based on superconducting transmon qubits. The best performing between these is *ibmq_santiago*. Its calibration data and properties are shown in Fig. 2.5, featuring:

- **Quantum volume**: a metric measuring the overall capabilities of a quantum computer, originally defined as the maximum size of the square circuit that can be executed successfully[38], a square circuit having the same number of qubits and depth. A competing definition has been proposed by IBM[39], related to the complexity of simulating the circuit with classical computation, that scales exponentially with its size.

¹IBM has recently retired this name with a rebrand, but it is still used to refer to the collective platform for experimentation created by the Quantum Lab and Composer.

- **Pending jobs:** the number of circuits that await to be run, sent from the users accessing the system. Usually, the queue makes up for most of the time needed to run a program on a device.
- **Basis gates:** the gates physically implemented on the computer.
- **CNOT and Readout error:** probability of failure for the execution of one of these operations, they are the main sources of error from gates.
- **T1:** known as the relaxation time, it is the time constant of the exponential probability distribution that describes the decay of a qubit from the excited state $|1\rangle$ to $|0\rangle$, mainly due to interactions with the environment.
- **T2:** called the dephasing time and analogous to $T1$, is the decay constant related to the loss of a qubit's phase, as in progressively evolving from $|-\rangle$ to an equal (classic) probabilistic mixture of $|-\rangle$ and $|+\rangle$. $T1$ and $T2$ are collectively known as the decoherence times.

5	Status: ● Online	Avg. CNOT Error: 6.616e-3
Qubits	Total pending jobs: 24 jobs	Avg. Readout Error: 1.840e-2
32	Processor type ⓘ: Falcon r4L	Avg. T1: 94.14 us
Quantum Volume	Version: 1.3.33	Avg. T2: 90.36 us
	Basis gates: CX, ID, RZ, SX, X	Providers with access: 1 Providers ↓

Figure 2.5: Properties of *ibmq_santiago* quantum computer.

When it comes to the physical implementation of a quantum computer, only some of the qubits can be connected by means of multi-qubits gates like *CNOT*. Thus, another important feature of a system is the topological diagram, also called connectivity map, visualizing the connections. For near-term applications, developing a circuit should always try to optimize the connections based on the ones of the systems available, since applying a gate between non-connected qubits is transpiled as a series of *SWAP* gates that introduce more noise. The connectivity map of *ibmq_santiago* is shown in Fig. 2.6, featuring a linear architecture. Additional informations regarding the single qubits and the error rate of the connections are color coded. The frequency of a transmon qubit is the energy needed to excite the ground state $|0\rangle$ to $|1\rangle$. In order to avoid thermal excitations, the systems must be operated at a much lower temperature than the thermal equivalent of the frequency, which in this case is below 250mK.

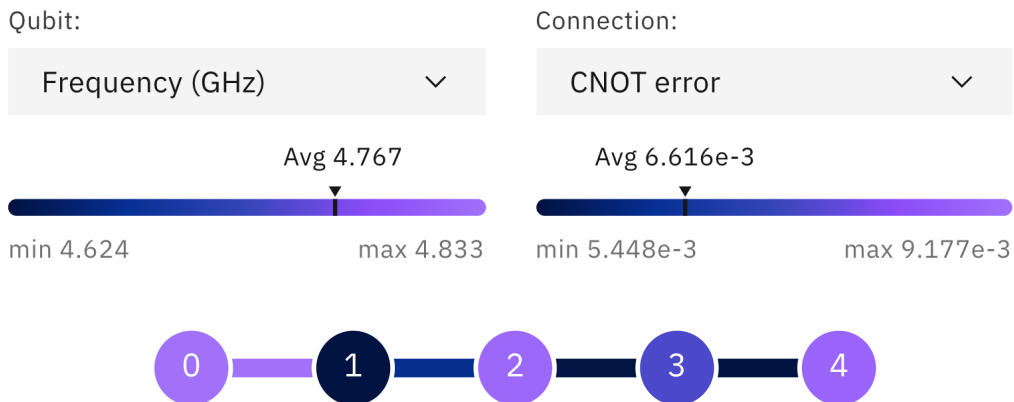


Figure 2.6: Topological diagram of *ibmq_santiago*.

Statevector simulator

Given the long time necessary to run a program on a real quantum computer and the destructive effects of errors and decoherence, it's important to make some tests when possible by employing various types of simulations. The *statevector* simulator computes the ideal performance of a circuit in a single shot by calculating the application of the unitary operators involved over the initial state.

QASM

A multi-purpose simulator and the main Qiskit Aer backend, the Quantum Assembly Simulator mimics the execution of circuits and measurements for a number of shots that can be chosen by the user, as well as many other parameters. The results obtained feature statistical fluctuations. An important feature of the QASM is the simulation of a realistic device. It is in fact possible to import the noise model, the connectivity map and the implemented gates list of the quantum computers featured on the platform.

2.3 Errors and decoherence

2.3.1 Limits of quantum hardware

The limited number of qubits, the possibility of gate error and decoherence are the main factors that define NISQ hardware, and pose significant limitations on the computations these devices can successfully execute. Decoherence is caused by the fact that the physical system implementing a qubit cannot be perfectly isolated by its environment, and interactions between the two irreversibly create a classical probabilistic mixture of states, instead of quantum superposition. Various types of physical implementations interact with different degrees of freedoms of the environment, and feature different decoherence times. However, in most cases this phenomenon still poses the main limit to the time complexity than any computation can achieve, since the circuit must be run in a much smaller timescale than the decoherence one.

The extents of errors and noise can be seen even by running a simple circuit such as the one of Fig. 2.3. The results of its execution for 1024 shots by the QASM, simulating a perfect circuit, and by *ibmq_santiago*, are written in Table 2.1. As can be seen, the limits of real hardware not only skew the distribution of measurements further than the simulation, but also generate counts in states that should not be accessible by the circuit.

Outcome	Ideal	QASM	<i>ibmq_santiago</i>
00	512	535	531
01	0	0	13
10	0	0	30
11	512	489	450

Table 2.1: Measurement outcomes for 1024 shots of the Bell state generating circuit (Fig. 2.3) for ideal case, QASM simulator and real quantum hardware.

2.3.2 Visualizing decoherence

Intuitively, a single-qubit mixed state can be seen as a point residing inside the Bloch sphere, since it is the "composition" of pure states corresponding to its surface. More quantitatively, since this mixed state can be represented by a 2×2 density matrix ρ , it can be written in terms of Pauli matrices as:

$$\rho = \frac{1}{2}(I + \mathbf{r} \cdot \boldsymbol{\sigma}) \quad (2.5)$$

where $\boldsymbol{\sigma}$ is the matrix vector given by (X, Y, Z) . Since the density matrix of a physical state must have unitary trace, it can be shown that $|\mathbf{r}| \leq 1$, and identify the state with the point in the Bloch sphere given by \mathbf{r} . Now, the interactions of a qubit with another system, such as the environment, can be expressed as a quantum operation, which is defined as being a trace-preserving map between two density matrices[40], in turn corresponding to remapping the Bloch sphere into itself by transforming \mathbf{r} accordingly. For example, at temperature $T = 0$ the decay from $|1\rangle$ to $|0\rangle$ described by the time constant $T1 = \tau$ corresponds to the transformation:

$$\begin{cases} r_x \rightarrow \sqrt{1-p}r_x, \\ r_y \rightarrow \sqrt{1-p}r_y, \\ r_z \rightarrow p + (1-p)r_z, \end{cases} \quad \text{where } p(t) = 1 - e^{-t/\tau} \quad (2.6)$$

with $p(t)$ being the probability of relaxation.

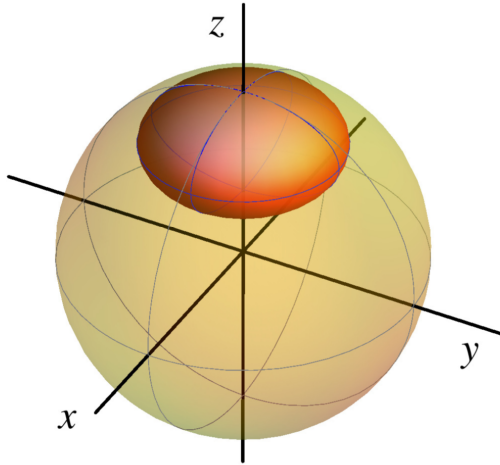


Figure 2.7: Effect of relaxation from $|1\rangle$ to $|0\rangle$ in the Bloch sphere representation.

The effect on the Bloch sphere is visualized in Fig. 2.7, progressively compressing it to the pole corresponding to $|0\rangle$. The dephasing related to $T2$ has an analogous effect, collapsing the sphere into the z axis. As can be seen, initially pure states quickly lose superposition and become harder to distinguish from each other.

2.3.3 Error correction

If errors arising from gates or decoherence can be reduced under a certain constant threshold, fault-tolerant quantum computation could be achieved[36]. The basic concept of error correction is that if a more complex system of gates executing the same operation of an existing one can be implemented obtaining an overall smaller error rate, then this process can be applied recursively to achieve an arbitrarily small error. Borrowing from classical computation, a possible implementation of error correcting codes features the use of redundancy, using more qubits to encode every term of a state², such as in $|0\rangle \rightarrow |000\rangle$, $|1\rangle \rightarrow |111\rangle$. As can be seen, quantum error correction is obtained using a vast amount of hardware resources, both in terms of qubits and gates, that in this moment are instead very limited, making its implementation infeasible for current applications. If quantum computers will become more scalable and feature a vast amount of qubits, as well as improved gates, the real potential of quantum computation could be accessible.

2.3.4 Error mitigation

Error mitigation aims to reduce the effects of errors without additional quantum resources. A standard method, easily implementable using Qiskit Ignis, is the State Preparation and Measurement Error Mitigation (SPAMEM). Based on the assumption that the same SPAM errors will be present in different circuits, for N qubits a $2^N \times 2^N$

²Differently from classical methods, redundancy is created by entanglement. As stated by the no-cloning theorem, it is impossible to simply copy the state.

calibration matrix M_Q needs to be computed[41]. The j -th column of the matrix is filled by preparing the possible j -th qubit state in the computational basis with a calibration circuit and measuring it for a number of shots, obtaining the frequencies of the possible outcomes. If the system is not prone to errors, M_Q is the identity matrix. Once the calibration is complete, it is possible to apply mitigation successfully to other circuits where SPAM is the prevalent source of errors. In a similar way, General Error Mitigation (GEM) can be achieved for a given circuit adding half of it and its reverse to the state preparation circuits of SPAMEM, computing one calibration matrix, repeating the process with the other half of the circuit and mediating the two matrices obtained. In either methods, given a vector of outcomes frequencies \mathbf{V} , it is possible to compute the mitigated outcomes \mathbf{X} by minimizing the least-square functional:

$$f(\mathbf{X}) = \sum_{i=1}^{2^N} (V_i - (M_Q \mathbf{X})_i)^2 \quad (2.7)$$

with the constraints $0 \leq X_i \leq 1$ and $\sum_{i=1}^{2^N} X_i = 1$.

2.4 The VQE algorithm

2.4.1 Variational quantum algorithms and the cost function

Even with the current limitations of quantum hardware, a notable class of algorithms based on a mixed quantum-classical approach is being developed, that may already be useful in many applications[42]. Variational quantum algorithms use classical optimizers to tweak a parametrized quantum circuit, called the ansatz or variational form, in order to find the minimum of a cost function that encodes a problem. Only the preparation of the state by the ansatz, which can be represented by a parametrized unitary $\hat{U}(\boldsymbol{\theta})$, and subsequent measurements are performed on a quantum device, while the rest of the computation is carried out classically, iteratively modifying the variational form until the minimum of the cost function or a stopping criteria is reached. Even if highly general, every cost function should satisfy some criteria regarding its properties:

- **Faithfulness:** the minimum of the function is the solution of the problem.
- **Estimation:** its value can be estimated efficiently by measuring the qubits.
- **Trainability:** the parameters $\boldsymbol{\theta}$ of the variational form can be optimized efficiently.

Where "efficiently" refers to the ability of performing the computation's steps in polynomial time. The Variational Quantum Eigensolver (VQE) is one of the first developed VQAs[12], aimed at finding the ground state of an hamiltonian \mathcal{H} and its energy E_G , and has already been used in numerous quantum chemistry and condensed matter applications. It is based on the variational principle:

$$\langle \psi(\boldsymbol{\theta}) | \mathcal{H} | \psi(\boldsymbol{\theta}) \rangle \geq E_G \quad (2.8)$$

Where the equality holds only when $|\psi(\boldsymbol{\theta})\rangle$, which is obtained from an initial state $|\psi_0\rangle$ by applying the variational form:

$$|\psi(\boldsymbol{\theta})\rangle = \hat{U}(\boldsymbol{\theta}) |\psi_0\rangle, \quad (2.9)$$

is the ground state. The hamiltonian may be generalized to a more generic cost function including additional constraints.

2.4.2 The ansatz

Ideally, the variational form should be able to generate any possible state of the Hilbert space spanned by the qubits, being able to encode any solution, but this would mean using an exponential number of parameters, quickly making the computation infeasible. Because of this, the ansatz must be written balancing the number of parameters and the portion of the Hilbert space that it can explore, which must still include or be in close proximity to the solution of the problem in exam. This is an open problem, and creating efficient variational forms is still mostly a heuristic effort. However, between the many possible approaches there can be distinguished two major categories.

Problem inspired

An intuitive approach to the construction of a variational form is trying to build it starting from the properties of the problem in exam. In quantum chemistry, the quantum Unitary Couple Cluster Single and Double excitations (qUCCSD) ansatz is one of the most accurate variational forms proposed[43]. Its circuit is obtained by the exponentiation of the electronic creation and annihilation operators for single and double excitations of the system, similarly to the simulation of the time evolution under a given hamiltonian. Even if it can achieve great accuracy and stability, the exponentiation of complex Pauli terms requires hardware resources still far from what is available in the NISQ era. Many other problem specific ansatze used in similar applications have been developed, trying to reduce the depth of the circuits needed by using methods such as the exponentiation of a limited number of terms of the hamiltonian[44].

Problem agnostic and hardware efficient

These variational forms only focus on modifying efficiently the initial state without considering specific properties of the problem in exam. An important type of problem agnostic ansatze are the hardware efficient ones, explicitly created to minimize the number of gates employed by the variational form by adapting it to the structure of a real device. Usually they are composed by a basic cell connecting two qubits that is layered in a "brick wall" like structure or repeated for improved convergence[45]. The number of repetitions or layers of a variational form is also referred to as its depth. Qiskit features a hardware efficient ansatz called *TwoLocal*, applying single qubits rotations followed by *CNOT* gates entangling the system in various possible configurations, one of which is shown in Fig. 2.8. Another common problem agnostic ansatz is *SO(4)*[46], connecting modules encoding all of the possible rotations in the space spanned by two qubits at a time.

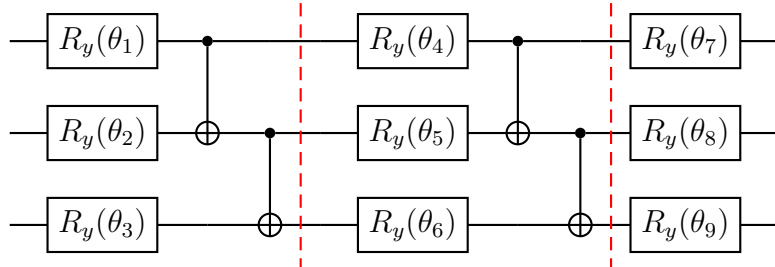


Figure 2.8: Example of TwoLocal ansatz with two repetitions, linear connections and R_y rotations over three qubits.

2.4.3 Optimizers

Many classical optimizers, some borrowed from machine learning methods, can be used when running a VQE, and may be essential in determining the convergence to the solution or the time required by program. The following are some of the common optimizers for VQEs available in Qiskit.

- **Gradient Descent:** a naive minimization routine, progressively updating the parameters in the direction of the negative gradient of the cost function, which must be provided or approximately measured with various method such as finite difference. The minimization can easily be trapped in local minima, but this algorithm serves as the basis for many other optimizers.
- **SLSQP-Sequential Least Squares Programming:** gradient based, it optimizes second order approximations of the function, also supporting constrained minimization both for equality and non-equality bounds. An example of its application is the least square problem of the error mitigation procedure described previously.
- **COBYLA-Constrained Optimization by Linear Approximation:** gradient free method that can resolve constrained minimization problems and evaluates the cost function just one time for iteration, is usually recommended for non smooth functions and constraints.
- **SPSA-Simultaneous Perturbation Stochastic Approximation:** this algorithm approximates the gradient evaluating the function only in two points at every iteration, regardless of the number of parameters. It is efficient for high dimensional problems with multiple unknown parameters, and can also be used in the presence of noise.

2.4.4 VQE and Qiskit

Finally, let's see how a standard VQE instance can be implemented using Qiskit. First of all, the modules are imported, then a quantum instance is constructed. The class *QuantumInstance* contains the configuration of the backend that will be used by an algorithm. In this case the QASM simulator is run in the Quantum Lab featuring the realistic model of *ibmq_santiago* with a randomly generated seed. A circuit will be evaluated 8000 times when reconstructing the state and the SPAMEM method *CompleteMeasFitter* is applied with 1000 shots in the computation of every column of the calibration matrix.

```
from qiskit import Aer
from qiskit.aqua import QuantumInstance
from qiskit.aqua import aqua_globals
from qiskit.providers.aer import QasmSimulator
from qiskit.providers.aer.noise import NoiseModel
from qiskit.ignis.mitigation.measurement import CompleteMeasFitter

IBMQ.load_account()
provider = IBMQ.get_provider(hub='ibm-q')
backend = Aer.get_backend('qasm_simulator')
device = provider.get_backend("ibmq_santiago")
coupling_map = device.configuration().coupling_map
noise_model = NoiseModel.from_backend(device)
basis_gates = noise_model.basis_gates
seed=aqua_globals.random_seed
QI=QuantumInstance(backend=backend, seed_simulator=seed, seed_transpiler=seed,
coupling_map=coupling_map, noise_model=noise_model, shots=8000,
measurement_error_mitigation_cls=CompleteMeasFitter, measurement_error_mitigation_shots=1000)
```

Then, the VQE is imported from the *aqua* library, as well as the optimizers and the variational form. Using these settings, TwoLocal implements the ansatz of Fig. 2.8. The VQE instance is defined using the ansatz and optimizer of choice, the quantum instance defined previously and a hamiltonian written with Qiskit's *Operator* class. Finally, the algorithm is run and the results are saved in a dictionary.

```
from qiskit.circuit.library import TwoLocal
from qiskit.aqua.components.optimizers import SLSQP, SPSA, COBYLA
from qiskit.aqua.algorithms import VQE

ansatz=TwoLocal(3,'ry','cx','linear',reps=2)
cob = COBYLA(maxiter=1000)
vqe = VQE(operator=Hamiltonian, var_form=ansatz, optimizer=cob, quantum_instance=QI)
result = vqe.run()
```

Chapter 3

VQE and the two-site model

Having introduced the fundamental tools of quantum computation, the VQE algorithm and the services offered by IBM Quantum Experience, this chapter will focus on the implementation of a specific VQE instance, finding the ground state of the two-site Bose-Hubbard model for small numbers of bosons and different values of the interaction energy.

3.1 Mapping the problem

3.1.1 Bosons to qubits

The first step in developing a quantum algorithm tackling a physical system is choosing how to translate its properties to the qubits representation. With fermionic systems, isomorphisms between the fermionic and spin-1/2 algebras such as the Jordan-Wigner, parity and Bravyi-Kitaev transformations[47][48] leverage the fact that the Fock space of M fermionic states and the M qubits space have the same dimension 2^M to express the creation and annihilation operators in terms of spin operators[49]. This is not possible in the case of bosons: since any number of particles can occupy the same state/site, the Fock space is infinite dimensional. However, approximate simulations of bosonic systems can still be achieved by truncating the space to a certain maximal occupation number for any state [50]. Since the bosonic creation and annihilation operators commutators are changed by restricting to a finite subspace:

$$[b_i, b_j] = 0 \tag{3.1}$$

$$[b_i, b_j^\dagger] = \delta_{ij} [1 - \frac{N+1}{N!} (b_i^\dagger)^N (b_i)^N] \tag{3.2}$$

an isomorphism between algebras is not achievable, and boson states with maximal occupation number N can be represented by n parafermions (qubits) only up to an error $\mathcal{O}(\frac{n}{N})$ [51]. However, systems conserving the total number of particles, such as the Bose-Hubbard model described in this thesis, naturally use only a fraction of the total Fock space. Therefore, it is possible to employ a one-to-one mapping between the bosonic and the qubit states[52]. An intuitive way to do this is to assign to each site a subset of m qubits capable of encoding its $N + 1$ possible occupation numbers.

The choice of encoding is essential in the determination of the resources required by the computation, a central aspect when dealing with NISQ limitations[53]. The bosonic operators of the j -th site can then be written in terms of Pauli matrices $\{I, X, Y, Z\}$ so that the creation and annihilation operators raise or lower the occupation number in the chosen encoding and multiply by the correct factor. The decomposition can be aided by thinking in terms of the computational basis projectors:

$$|1\rangle\langle 1| = \frac{I - Z}{2} \quad (3.3)$$

$$|0\rangle\langle 0| = \frac{I + Z}{2} \quad (3.4)$$

$$|0\rangle\langle 1| = \frac{X + iY}{2} \quad (3.5)$$

$$|1\rangle\langle 0| = \frac{X - iY}{2} \quad (3.6)$$

and is limited to the m qubits of the j -th subspace. These operators can then be composed (trivially if they act over different sites) to write the problem's Hamiltonian or other observables as a sum of Pauli strings.

3.1.2 Unary encoding

Remembering that the second quantization hamiltonian of the two site Bose-Hubbard model is:

$$H = -J(b_R^\dagger b_L + b_L^\dagger b_R) + \frac{U}{2}[\hat{n}_R(\hat{n}_R - 1) + \hat{n}_L(\hat{n}_L - 1)] \quad (3.7)$$

Since the number of bosons in one well is always determined by the one in the other, the problem can be reduced to encoding the $N + 1$ possible states as counting the occupations of a single site. The simplest way to do this is by using the unary encoding, where a number is represented by the position of the only 1-valued bit in a $N+1$ length string of otherwise 0-valued qubits, as in:

$$\begin{aligned} |1000\dots0\rangle &\leftrightarrow |0, N\rangle \\ |0100\dots0\rangle &\leftrightarrow |1, N-1\rangle \\ |0010\dots0\rangle &\leftrightarrow |2, N-2\rangle \\ &\vdots && \vdots \\ |0000\dots1\rangle &\leftrightarrow |N, 0\rangle \end{aligned}$$

This encoding is extremely inefficient in terms of the number of qubits used, but can straightforwardly be extended to any N . Furthermore, since the operators $b_R^\dagger b_L$ and $b_L^\dagger b_R$ always correspond to moving the 1-valued qubit one position to the right or to the left, the number of multi-qubit gates involved in the quantum circuit simulating the hamiltonian is much smaller than with other encodings. To simplify the notation, identity matrices involved in the $N + 1$ fold tensor product are dropped, and tensor product is implied in the composition of terms referring to different qubits, as in:

$$I \otimes Z \otimes X \otimes I \otimes I \leftrightarrow Z_1 X_2$$

Also, since we are not interested in the actual value of the fundamental state's energy, the terms proportional to the identity in the expansion of the Hamiltonian can be neglected. Let's start from the number operator:

$$\hat{n}_L = \sum_{j=0}^N j \frac{I_j - Z_j}{2} \quad (3.8)$$

Since $\hat{n}_L = N - \hat{n}_R$:

$$\hat{n}_R(\hat{n}_R - 1) + \hat{n}_L(\hat{n}_L - 1) = 2\hat{n}_L(\hat{n}_L - N) + N^2 - N \quad (3.9)$$

$$2\hat{n}_L(\hat{n}_L - N) = \sum_{j=0}^N j(N-j)(Z_j - I_j) \quad (3.10)$$

While, for the hopping terms, given:

$$b_R b_L^\dagger = \frac{1}{4} \sum_{j=0}^{N-1} \sqrt{j+1} \sqrt{N-j} (X_j + iY_j)(X_{j+1} - iY_{j+1}) \quad (3.11)$$

$$b_L^\dagger b_R = (b_R b_L^\dagger)^\dagger \quad (3.12)$$

The Hamiltonian can then be written as:

$$H_{PauliUnary} = -\frac{J}{2} \sum_{j=0}^{N-1} \sqrt{j+1} \sqrt{N-j} (X_j X_{j+1} + Y_j Y_{j+1}) + \frac{U}{2} \sum_{j=0}^N j(N-j) Z_j \quad (3.13)$$

3.1.3 Gray encoding, N=3

More compact ways to count m different occupation numbers are the standard binary and the Gray code, which use only $\lceil \log_2 m \rceil$ qubits. The Gray code, also called reflected binary, is of special interest because moving between adjacent integers always requires only one qubit flip at time, simplifying the creation-annihilation operators expansion to Pauli strings with respect to the standard binary encoding. However, counting to higher numbers requires progressively more complex compositions of projectors over all of the qubits. The Gray code mapping of the $N = 3$ case uses only two qubits :

$$\begin{aligned} |00\rangle &\leftrightarrow |0, 3\rangle \\ |01\rangle &\leftrightarrow |1, 2\rangle \\ |11\rangle &\leftrightarrow |2, 1\rangle \\ |10\rangle &\leftrightarrow |3, 0\rangle \end{aligned}$$

$$b_R b_L^\dagger = \frac{1}{4} \left[\sqrt{3}(I + Z)(X - iY) + 2(X - iY)(I - Z) + \sqrt{3}(I - Z)(X + iY) \right] \quad (3.14)$$

$$2\hat{n}_L(\hat{n}_L - N) = -4(|11\rangle \langle 11| + |01\rangle \langle 01|) = 2(IZ - II) \quad (3.15)$$

and the Hamiltonian has an exceptionally simple form:

$$H_{PauliGray} = -J(\sqrt{3}IX + XI - ZX) + U(IZ) \quad (3.16)$$

3.2 Ansatze

Choosing the correct ansatz is extremely important in the implementation of the VQE, as the parametrized circuit must be able to create qubit states as close to the solution as possible. This can be aided by tayloring the ansatz to known symmetries or properties of the system. Using the unary encoding in the $N=2$ case, all the states with physical meaning can be written as a linear combination of $|001\rangle$, $|010\rangle$ and $|100\rangle$ with real coefficients. A possible ansatz is then given by the generalization of the circuit generating the *W-Bell* state[54]:

$$|W_{Bell}\rangle = \frac{|001\rangle + |010\rangle + |100\rangle}{\sqrt{3}} \quad (3.17)$$

by means of controlled- R_y gates, obtaining the circuit shown in Fig. 3.1, which can describe all the possible states of interest with the minimum number of parameters.

$$|\psi(\theta_1, \theta_2)\rangle = \cos\left(\frac{\theta_1}{2}\right)|100\rangle + \sin\left(\frac{\theta_1}{2}\right)\left[\cos\left(\frac{\theta_2}{2}\right)|010\rangle + \sin\left(\frac{\theta_2}{2}\right)|001\rangle\right] \quad (3.18)$$

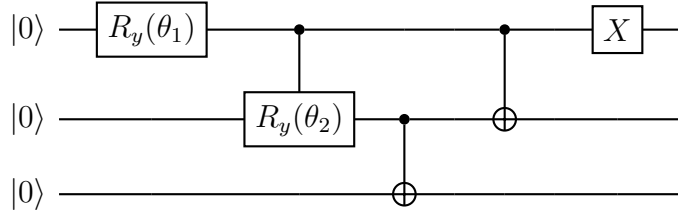


Figure 3.1: Unary ansatz for $N = 2$.

The ansatz can be straightforwardly extended to any unary encoded case, as in Fig. 3.2 for $N=4$, and is the one used in the following VQE instances. Another important factor in the implementation is that symmetries of the system might be used to reduce the required number of qubits[55], but they can also be directly implemented in the variational form by constraining some of the parameters. For example, the symmetry between sites:

$$\langle \hat{n}_L \rangle = \langle \hat{n}_R \rangle \quad (3.19)$$

limits the actual degrees of freedom to $\lfloor N/2 \rfloor$. Instead of imposing Eq. 3.19 after the computation, the ansatz can be suitably modified by changing the order of the connections and constraining the parameters by considering Eq. 3.18 and its generalizations.

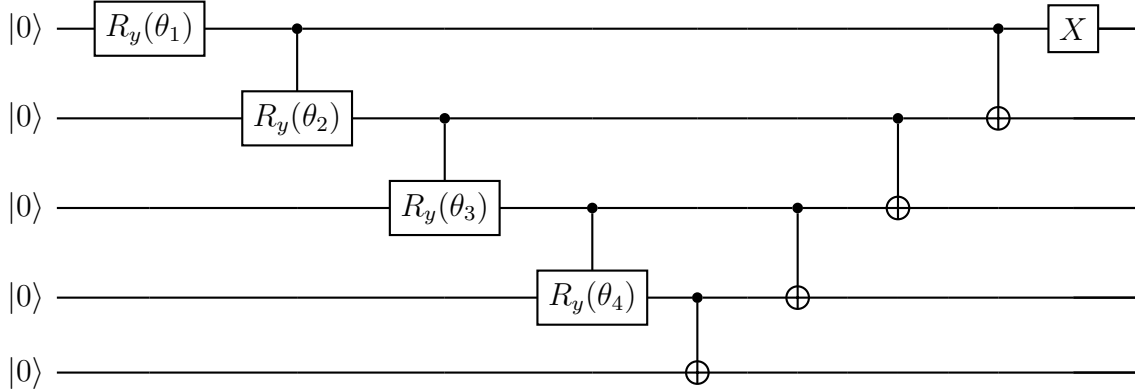


Figure 3.2: Unary ansatz for $N = 4$.

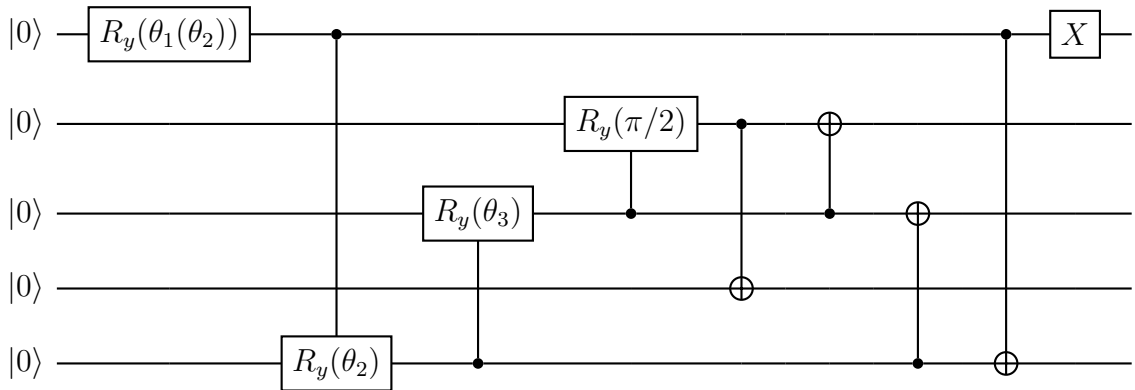


Figure 3.3: Symmetrized unary ansatz for $N = 4$.

Since qubit connections are limited in a real quantum computer, one can instead change the qubit ordering by explicitly assigning them to the virtual ones, but this is usually automatically taken care of by the circuit transpiler algorithm. An example for $N=4$ is shown in Fig. 3.3, where:

$$\theta_1 \rightarrow \theta_1(\theta_2) = 2 \operatorname{arccot} \left(\cos \frac{\theta_2}{2} \right) \quad (3.20)$$

Since the Gray code $N = 3$ case uses efficiently all of the qubit states, the simulations will be run using hardware efficient ansatze such as TwoLocal or the simple circuit shown in Fig. 3.4, which ensures the symmetry between states.

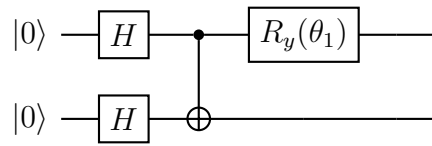


Figure 3.4: Gray encoding, symmetric ansatz for $N = 3$.

3.3 VQE simulations and measurements

3.3.1 Statevector simulations

Before running any algorithm on a real quantum computer, it is important to check if the known outcomes match the ones obtained with the simulation of a perfect circuit, proving the validity of the mapping and the ansatz. This can be done by using Qiskit's statevector simulator. Since we are interested in the many-body properties and quantum correlations of the system, the goal of the algorithm is to replicate the exact values of the entanglement entropy and coherence visibility by finding the ground state for different values of the interaction energy term U , normalized by the hopping term $J = 1$. To check whether the VQE finds results comparable with the ones from direct diagonalization, it is also useful to compute the state fidelity and the energy difference between the known solution and the quantum one. The results for $N = 3$ are shown in Fig. 3.5, being perfectly compatible with the exact values for $U > 0$, but differing greatly for some values of the attractive interaction case.

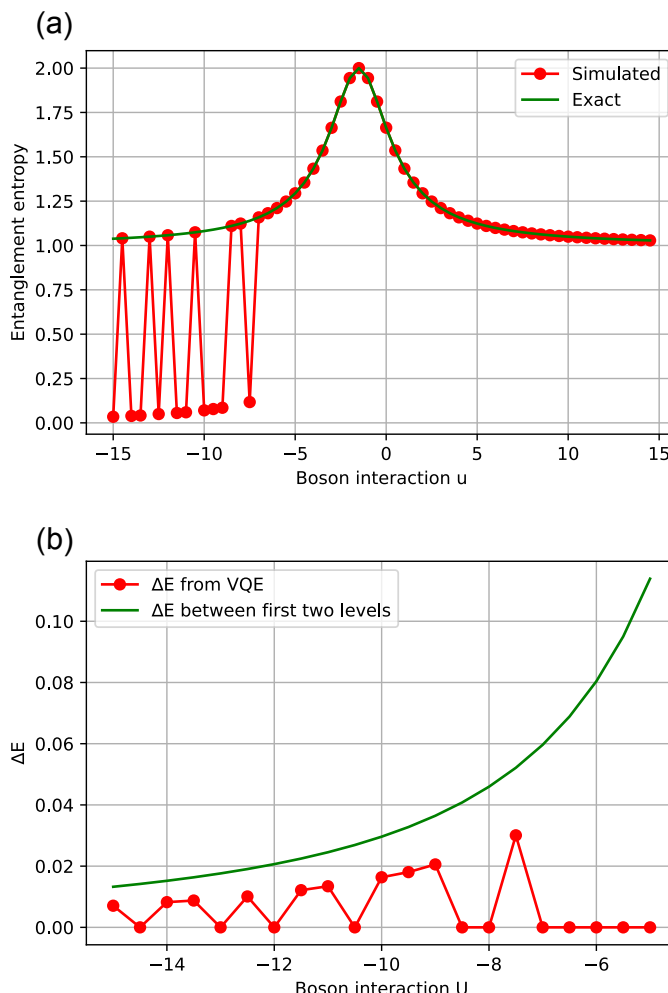


Figure 3.5: (a) $N = 3$ entanglement entropy values for the first statevector simulation, (b) energy residuals and difference between ground and first excited state energies.

This is due to the fact that the first two energy levels become really close for $U < 0$ and also feature almost the same probabilities for the occupations, but in the first excited state half of them have opposite relative phase. Thus, an equal superposition of these two is a state of almost fundamental energy where all of the bosons are essentially entirely localized in one of the two sites instead of being symmetric. This creates a very strong local minimum that easily traps the minimization algorithm. Also, to aid the convergence of the VQE, boson interaction is progressively increased and the optimal parameters of the previous step are passed as the starting point of the next one, which could result in starting too close to this or other local minima. Using the symmetric ansatz, the local minimum is erased and the calculations always reach the correct energy values. Since we are interested in the insulator to superfluid transition, which always takes place for repulsive interactions, the next simulations will focus on the range $U \in [0, 10]$. The previous considerations are still worth noting, since they show how quantum computation could aid the study of very fragile states, otherwise nearly impossible to replicate, such as the Schrödinger's cat state[56]. Similar considerations also stand for $N=4$, while for $N=2$ and for the Gray coded case simulations always reach the exact results even without symmetrization. Overall, statevector simulations of symmetric ansatze always provide energy values with $\sim 10^{-7}$ accuracy (Fig. 3.6).

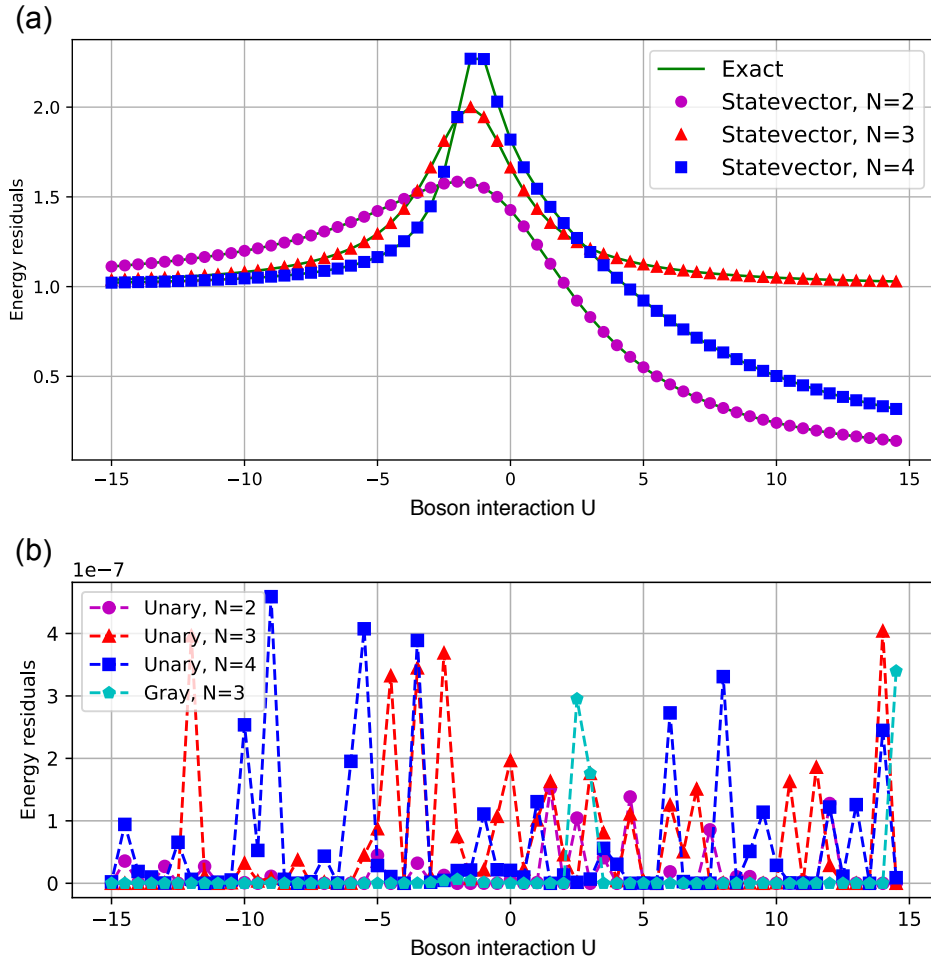


Figure 3.6: (a) Statevector simulations with symmetric ansatze, (b) energy residuals.

3.3.2 Unary coding, simulations with noise

The next step is to study how the limitations of real quantum hardware may affect the computation and what methods can be used to reduce their effects. This has been done importing to the QASM simulator the noise model, the connection map and the implemented gates list of *ibmq_santiago*. The device was chosen for having the best performing gates and linear connections between its five qubits, making the implementation of all the unary ansatze possible. The classical optimizer used in the simulations is COBYLA, since it gives both the most accurate results and fastest convergence time with respect to the other ones. To really see the extent of the effects of noise over the accuracy, the first simulation for $N = 3$ has been run without any form of noise mitigation, while all the other ones will be using the SPAMEM method *CompleteMeasFitter*. As can be seen in Fig. 3.7, even if the mitigation method greatly improves the results, they are still far from being compatible with the known solution. This great difference is due to the fact that noise and gate errors generate counts in all of the qubit states which have no physical meaning (have more than one qubit in $|1\rangle$), even if they could not in theory be accessed by the ansatz. Since these counts are generated by noise, introducing further constraints in the ansatz or in the problem hamiltonian is not as useful as in other cases[57].

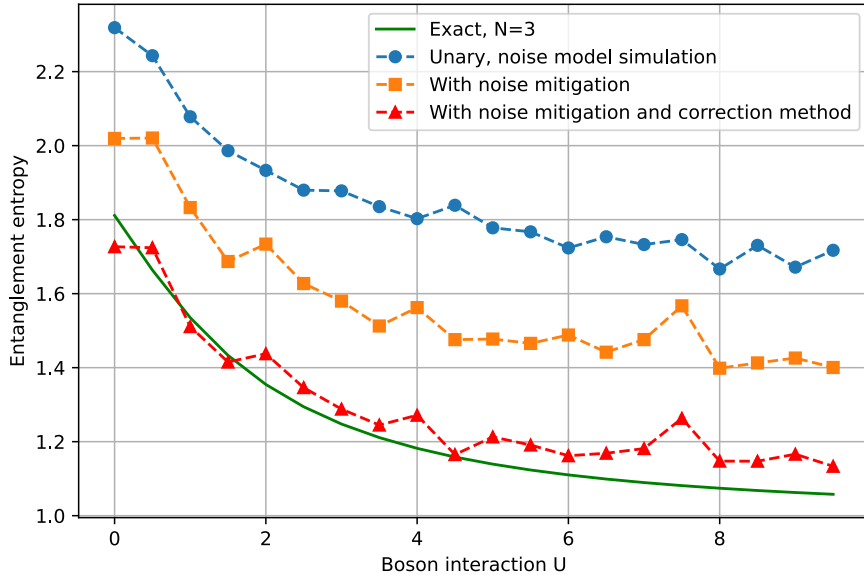


Figure 3.7: Noise reduction and correction applied to a noisy simulation for $N = 3$.

A possible solution might be to modify the VQE so to project the state generated by the ansatz over the subspace of the qubit states which are of interest, then measuring the energy over the resulting density matrix. A very simple, but *a posteriori*, way to solve this problem is instead to only consider the counts in the states of interest and discard all the others. Even if quite rudimental, this technique still improves the results greatly and the "reduced" states are consistently closer to the correct ones.

Noise introduces significant systematic errors, much greater than the statistical ones. In fact, the standard deviation over the found energy values can be accessed by implementing a callback function which saves the intermediate results of the VQE, but this values do not exceed $\sigma = 0.03$, while differences between the real ground state energies and the expectation values of the hamiltonian over the reduced states are usually three to ten times greater. Because of this, only a qualitative description of the results will be given, and values of the quantities in exam are reported without error bars, assuming that the systematic ones always dominate the statistical. Moreover, energy residuals might not be the best indicator of correspondence with the solutions, due to the fact that the variational principle is invalidated by the presence of counts in non-physical states. Observing the fidelities of the computed states, it is found that symmetric ansatze with optimal connections comparatively perform worse than the standard ones, probably because more parameters may help in the noisy environment. In VQE instances, increasing the ansatze depth by repeating their basic circuit usually improves convergence, but in this case this would ruin their properties, since they are not problem-agnostic. Since the mean fidelity values of Fig. 3.8 for the same N might still be statistically compatible the difference is subtle, but common to all of the three cases studied.

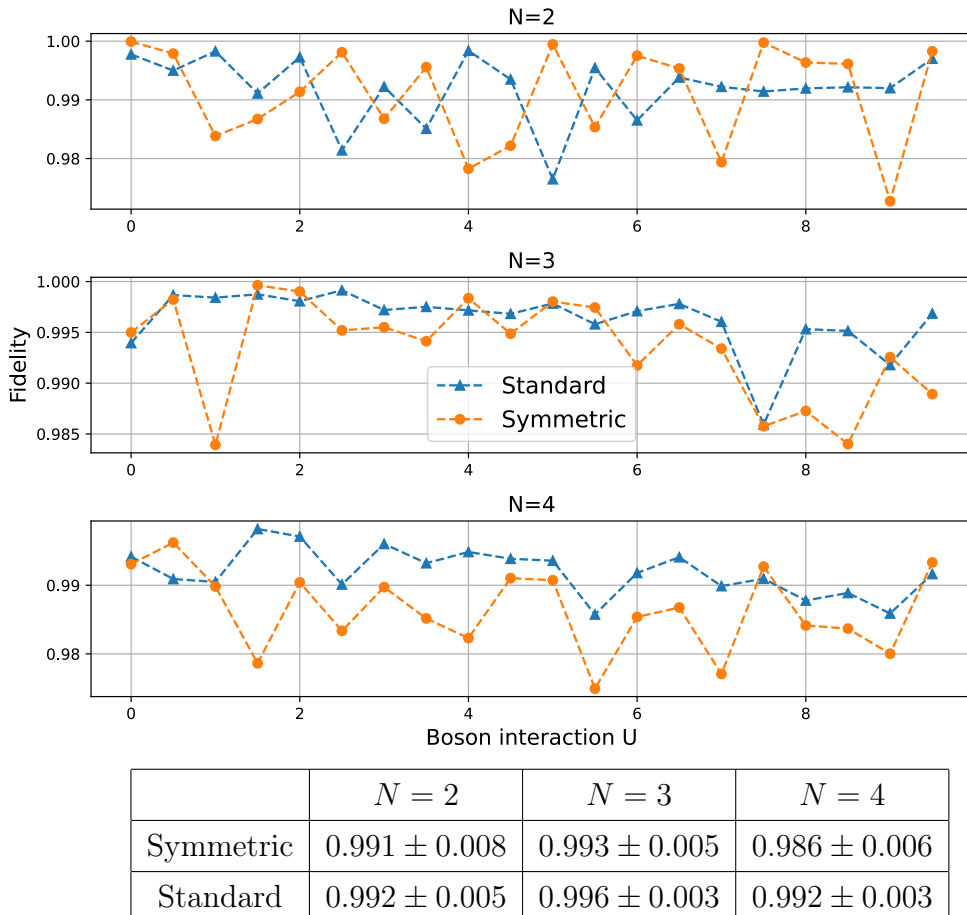


Figure 3.8: Compared fidelities between standard and symmetrized unary ansatze. The table shows the fidelities means with standard deviations.

Quantities regarding the quantum correlations are computed starting from the probabilities of the reduced states. Adding auxiliary operators to the VQE to measure observables like the coherence visibility would be of no use: without the post processing operations, states would have no physical meaning. Even if systematic errors make the numerical accuracy hard evaluate and introduce significant deviations, the resulting values still qualitatively follow the exact solutions and can be distinguished from one another.

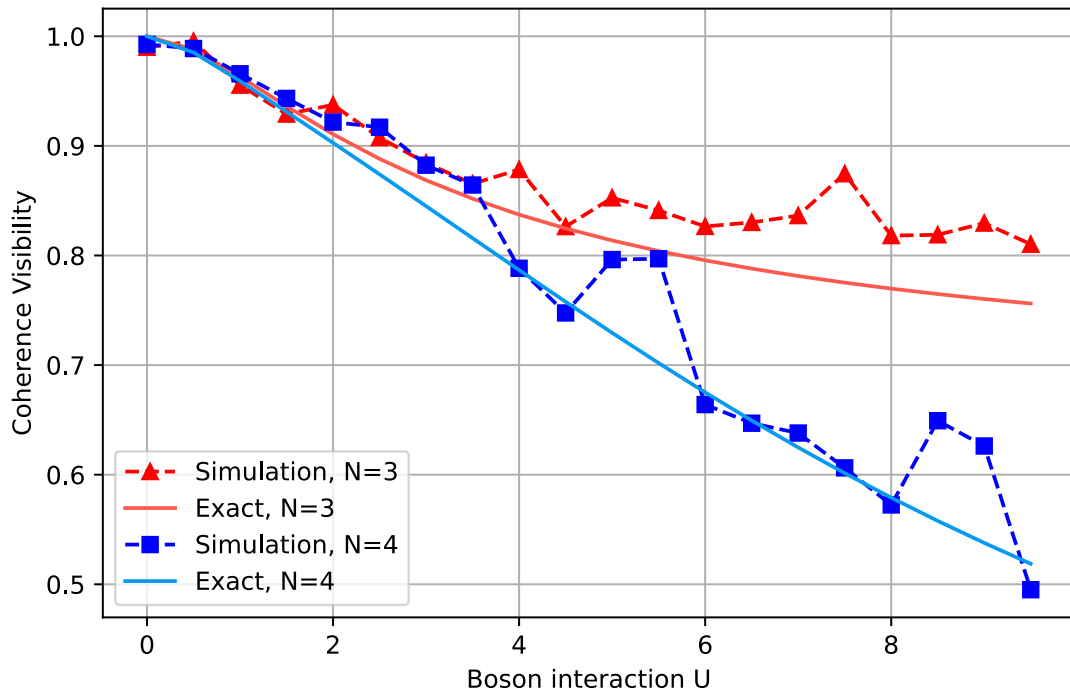


Figure 3.9: Computed visibility for noise model simulations with unary ansatze.

Most notably, the difference between cases with N commensurate to the number of sites and those with odd N , crucial to the existence of the quantum phase transition, is discernible both by graphing the entanglement entropy (Fig. 3.10) and the visibility (Fig. 3.9). The extent of systematic errors is apparent by plotting the residuals of the entanglement entropy (Fig. 3.10), which show how the exact values are constantly overestimated by the noisy simulations. This may be partially due to the fact that noise-generated counts proportionally affect more the physical states with lower probability of measurement, which are suppressed by the increasing repulsive interaction, and might become the predominant error factor for higher values of U . Even with the range of interactions used, this effect can be seen as the tendency of the residuals for $N = 3$ to increase.

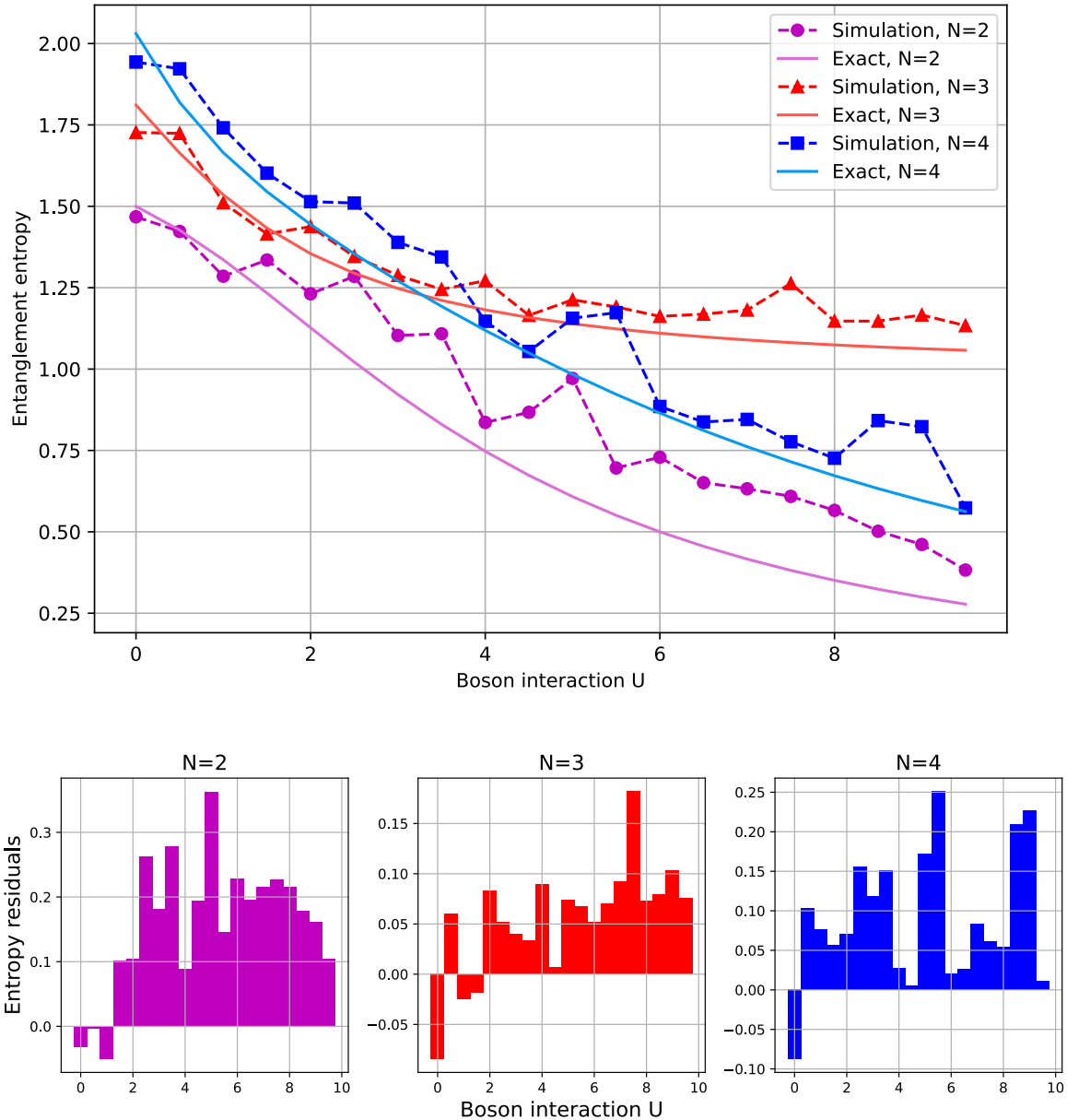


Figure 3.10: Entanglement entropy values and residuals from noise model simulations of various occupation numbers with unary ansatze.

3.3.3 $N=3$, Unary vs. Gray

Even if easily scalable and theoretically requiring less gates when implementing a quantum simulation of more complex systems, this properties of the unary encoding might still be overwhelmed in NISQ applications by the fact that the number of states without physical meaning grows exponentially faster than the useful ones when encoding more bosons for any site, with noise generating counts in all of them even with problem

specific ansatze. The compact Gray encoding uses all of the possible qubit states when $N - 1$ is a power of two, both eliminating the need for correction methods as the one used before and greatly reducing the number of qubits used. Noisy simulations of the Gray encoded $N = 3$ case have been performed using the TwoLocal ansatz at different depths and the symmetric simple ansatz of Fig. 3.4. Standard error mitigation has been applied.

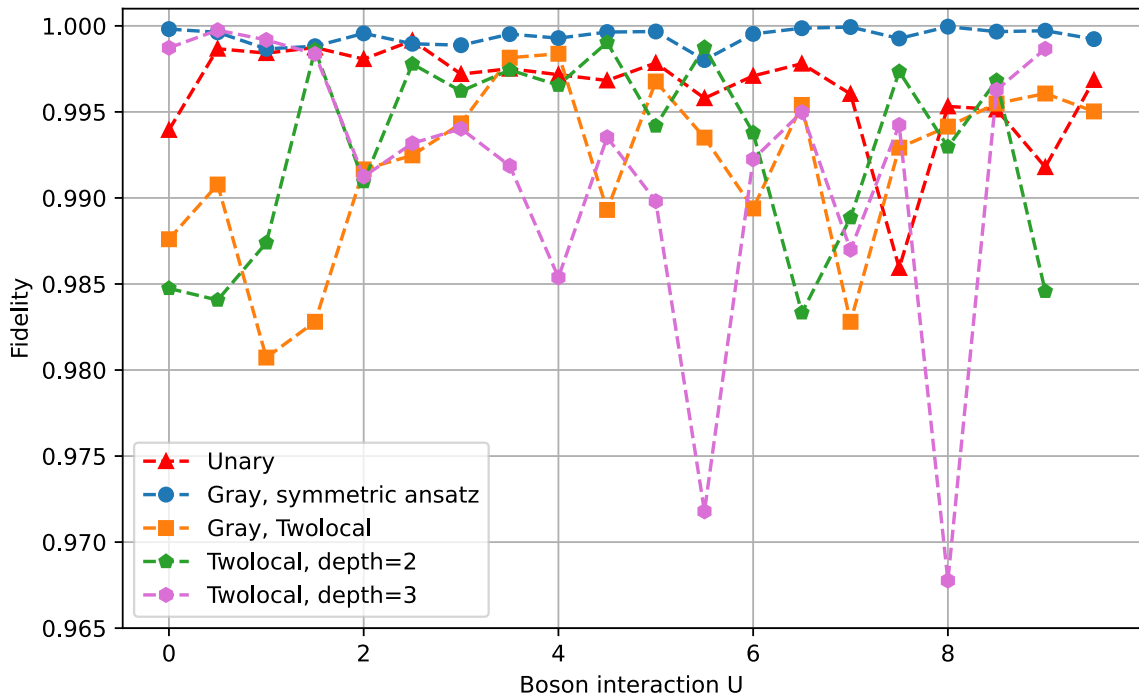


Figure 3.11: Fidelities for various ansatze, $N = 3$.

As can be seen in Fig. 3.11, repeating the TwoLocal ansatz does not seem to improve performance, probably because the problem is so simple that the added gates just introduce more noise, with $depth = 1$ and $depth = 2$ TwoLocal circuits achieving fidelities comparable to, but slightly worse than the unary simulation. The symmetric ansatz performs significantly better than any other implemented instances. Remarkably, some of the energy values are even statistically compatible with the actual ones. By the variational principle, this means that also the found states, hence other quantities, are compatible with the analytic solution, but for the majority of the results systematic errors are still predominant. Another important feature of the Gray coding is a significant speed up of the computation time, which is usually halved with respect to the unary coded simulations. Even if fidelities for the TwoLocal $depth = 1$ simulations are lower than for the unary case, computed values both for the entanglement entropy and the visibility are closer to the exact ones, as can be seen by plotting the residuals, which are practically the same for the two metrics.

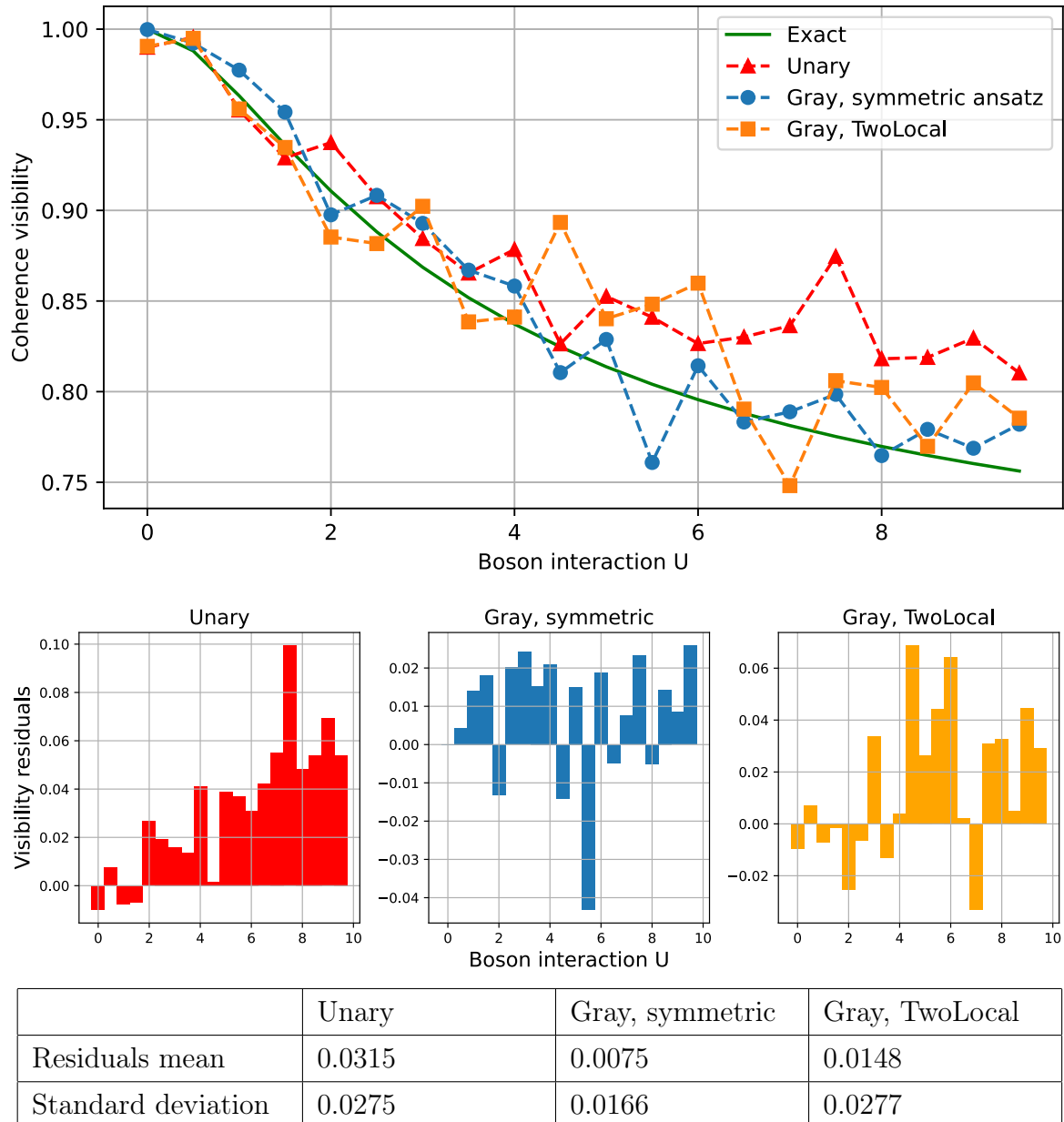


Figure 3.12: Coherence visibility values and residuals from noise model simulations of $N = 3$ with best performing ansatze. The table shows the means and standard deviations of the residuals.

The overall results are still affected for the major part by systematic errors, usually overestimating the curves, but accuracy does not seem to worsen at higher U using the Gray code (Fig. 3.12). Using only two qubits, the symmetric ansatz provides the overall best performance, both in terms of computation time and accuracy, so it will be used in the run on quantum hardware. For a possible extension of the studied system to a larger number of sites, NISQ simulations of low occupation numbers might be achieved coding three bosons for site with the Gray code.

3.3.4 Quantum hardware measurements

Finally, the simple symmetric Gray code VQE is run on a real quantum computer, using two qubits of `ibmq_santiago` with the classical optimizer COBYLA. Since the run must test if the actual quantum hardware can compute the solution, the ansatz's parameters initial point has been randomized. To improve the results, a second run is done using the optimal points of the first one as starting parameters, and the final results are obtained choosing the values with minimum energy between the two. It is worth noting that recently IBM Quantum has introduced *QiskitRuntime*, a new architecture that can significantly speed up the computation of standard quantum programs requiring many iterations, but at this time the VQE instance offered only features the SPSA and QNSPSA optimizers, in this case performing far worse than COBYLA both in terms of number of evaluations required for convergence and accuracy.

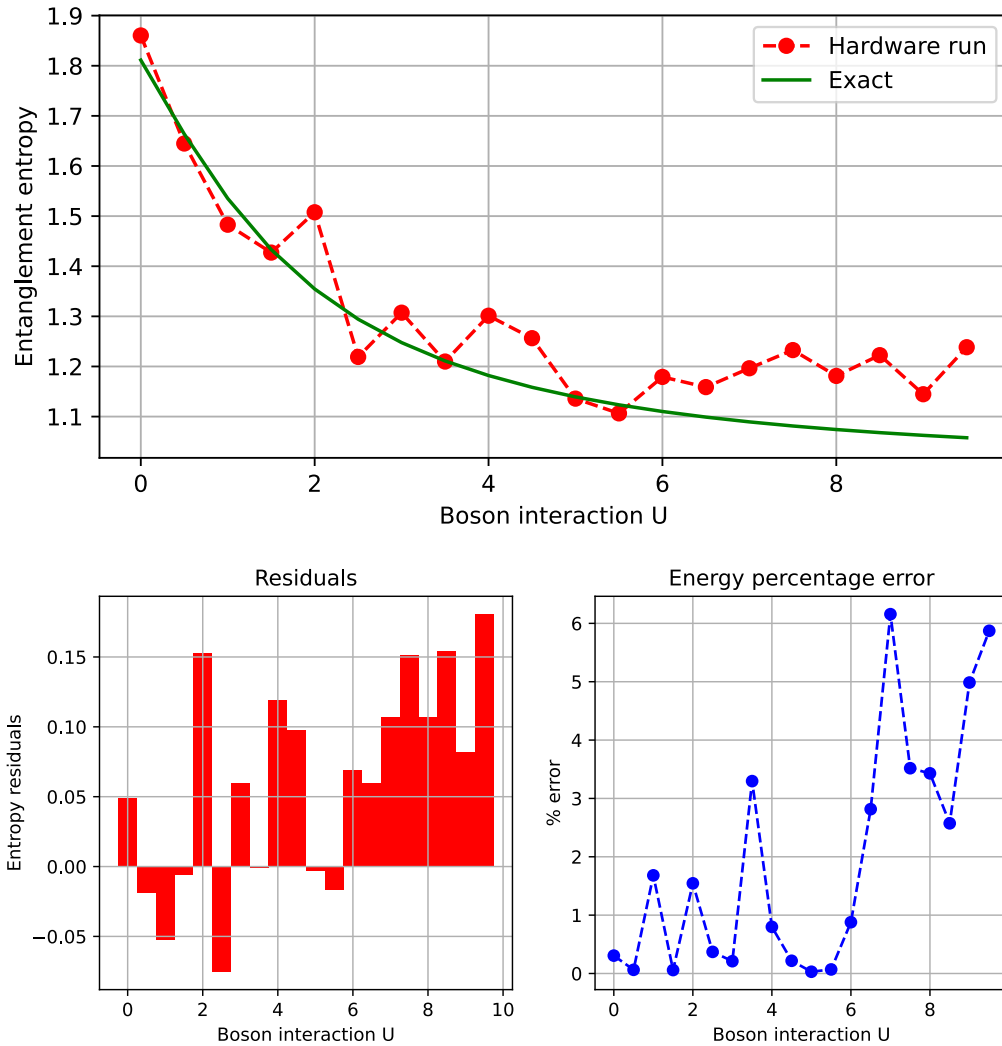


Figure 3.13: Best entanglement entropy values, residuals and relative error for the ground state energy, selected from two hardware runs using the symmetric Gray code ansatz for $N = 3$.

The results are summarized in Fig. 3.13, where the entanglement entropy and its residuals are plotted together with the relative error of the energies found by the algorithm with respect to the exact ones. As can be seen, residuals resemble the ones obtained from noise model simulations of the unary ansatz in Fig. 3.10, showing a tendency to increase for larger interaction values, also common to the relative deviation from the ground state energy. Overall, accuracy is worse than what expected from the simulations, but the shape of the curve is still qualitatively outlined and some of the values are really close to the exact entanglement entropy. It could be argued that, iterating the computation more times and progressively selecting the results with minimum energy, an accurate description of the ground state can be provided for small values of $U < 6$ purely by the quantum-classical algorithm.

Conclusion

Results

The ideal simulations show how the VQE is theoretically able to perfectly replicate the results given by exact diagonalization, but is limited by the noise and error rate of current quantum computers. Apart from the prevalence of systematic errors, quantifying the accuracy of the results achieved in these computations is not straightforward, since the VQE implemented in Qiskit can only recover uncertainties on the computed energies. Even if by leveraging the variational principle it can be argued that statistical compatibility with the ground state energy corresponds to compatibility with the ground state itself, there is no way to extract only from this values the uncertainties on the single probabilities for the possible occupations, which are used to compute the metrics for quantum correlations. Moreover, this is only possible when all the qubit states are mapped to the occupation ones, or if states with non physical meaning cannot be accessed by the computation, otherwise the variational principle would be invalid, as in the case of the unary encodings. Since quantifying the accuracy of the results is still useful, it is necessary to introduce an experimental criterium. In this case, I have decided to consider numerical accuracy as a less than 5% deviation from the exact values of the metrics, computed with respect to their total excursion in the range of interactions considered. This should isolate the results which can at least faithfully replicate the shape of the quantities of interest, differentiating between the possible many-body behaviours of the system. The relative errors for the best entanglement entropy values obtained are shown in Table 3.1. The hardware run with N=3 was executed using the Gray code mapping and a symmetric ansatz, while for N=2,4 the computation was carried out with noise model simulations, employing unary mapping and non-symmetric ansatze. It should be noted that the simulated outcomes underestimate the extent of errors of the real quantum computer, since the noise model doesn't account for errors when preparing the qubits in $|0\rangle$ and only considers decoherence effects related to relaxation and dephasing, while they may be other kinds of interactions with the environment or errors that violate the locality of the operations and introduce correlations between the qubits[58]. The range covered by the entanglement entropy increases with the number of bosons involved, generally improving the relative accuracy accordingly. For the same reason, coherence visibility might not be a useful metric in these imperfect computations, since its range is smaller and bound to be between one and zero for any number of bosons, highlighting deviations and making it harder to discern the different cases qualitatively.

Boson interaction (U)	Hardware, N=3	Simulation, N=4	Simulation, N=2
0.00	6.52	5.96	2.64
0.50	2.52	7.03	0.33
1.00	6.95	5.21	4.14
1.50	0.79	3.87	8.30
2.00	20.32	4.77	8.53
2.50	9.99	10.61	21.53
3.00	7.92	8.06	14.84
3.50	0.16	10.31	22.76
4.00	15.84	1.90	7.26
4.50	13.01	0.32	15.85
5.00	0.46	11.74	29.71
5.50	2.26	17.09	11.91
6.00	9.15	1.37	18.75
6.50	7.94	1.78	15.99
7.00	14.20	5.71	17.67
7.50	20.10	4.18	18.60
8.00	14.20	3.66	17.59
8.50	20.51	14.23	14.57
9.00	10.89	15.45	13.23
9.50	23.97	0.77	8.58

Table 3.1: Computed entanglement entropy percentage errors for different numbers of bosons and repulsive interaction intensities in the two-site model. Deviations less than 5% are highlighted in blue.

The genuine quantum correlations of the systems are hard to replicate, and these mostly inaccurate values were obtained while achieving fidelities with the true ground states usually superior to 0.98. However, for the hardware run a quarter of the results still satisfy the accuracy criterium, and they do so with very small deviations, which are also really different from the rest of the errors. This may suggest that, at least for small interaction values and using the Gray mapping, the inaccuracies are due to specific fluctuations or sub-optimal convergence of the single VQE instance and could be leveled out reiterating the algorithm. Overall, the compact Gray encoding proves to be far superior to the unary, both in terms of accuracy and computation time, even if its properties can be only fully exploited when dealing with a number of possible states which is a power of two and requires progressively more complex decompositions when dealing with more bosons.

Finally, even if the exact values couldn't be exactly replicated, it is still possible to qualitatively discern the difference in behavior between integer filling factors ($N=2,4$) and non-commensurate number of bosons ($N=3$), which is one of the major aspects that must be considered when investigating the many-body properties of the Bose-Hubbard model.

Next steps

In these concluding remarks, I would like to address the natural prosecution of this work. Its realization would be extending the quantum variational approach to the Bose-Hubbard model to a greater number of sites, trying to replicate its many-body properties for conserved total particles number and integer filling factors. The two-site model considered in this implementation of the VQE can be seen as a single cell or site in a bigger simulation, and may have offered some insights into what mappings and ansatze could be used when dealing with the limitations of the NISQ era. The results obtained strongly suggest that a viable near term extension of the model should use a compact encoding, such as the Gray code, when counting the number of bosons in every site. For example, studying the transition at unitary filling might require only two qubit per site, since even when the number of particles in one of them fluctuates maximally, as in the superfluid state, from the poisson distribution can be inferred that a maximum occupation of only three bosons is required to consider $\sim 95\%$ of the possibilities. As for the ansatz, it could either be developed to automatically preserve the total number of particles, or employ a problem agnostic approach, encoding the conservation rule as a constraint in the hamiltonian. However, as shown in this work the implementation of an optimal VQE is not a straightforward and algorithmic process but requires many heuristic considerations, proceeding almost by trials. Nevertheless, the interest sparked by VQAs resides in the fact that they seem to finally be able to address practical problems and physical systems with current and near-term quantum computers.

Bibliography

- [1] M. Greiner, O. Mandel, T. Esslinger, T. W. Hänsch, and I. Bloch, *Quantum phase transition from a superfluid to a Mott insulator in a gas of ultracold atoms*, Nature **415**, 39–44 (2002).
- [2] D. S. Grun, L. H. Ymai, K. W. Wilsmann, A. P. Tonel, A. Foerster, and J. Links. *Integrable atomtronic interferometry*, (2020).
- [3] A. Hamma, F. Markopoulou, S. Lloyd, F. Caravelli, S. Severini, and K. Markström, *Quantum Bose-Hubbard model with an evolving graph as a toy model for emergent spacetime*, Physical Review D **81** (2010).
- [4] D. Deutsch, *Quantum Theory, the Church-Turing Principle and the Universal Quantum Computer*, Proceedings of the Royal Society of London. Series A, Mathematical and Physical Sciences **400**, 97–117 (1985).
- [5] P. W. Shor, *Algorithms for quantum computation: discrete logarithms and factoring*, Proceedings 35th Annual Symposium on Foundations of Computer Science **1**, 124–134 (1994).
- [6] D. P. DiVincenzo, *Topics in Quantum Computers*, Mesoscopic Electron Transport **345**, 657–677 (1997).
- [7] I. L. Chuang, N. A. Gershenfeld, and M. Kubinec, *Experimental Implementation of Fast Quantum Searching*, Physical Review Letters **80**, 3408–3411 (1998).
- [8] M. S. Underwood and D. L. Feder, *Bose-Hubbard model for universal quantum-walk-based computation*, Physical Review A **85** (2012).
- [9] F. Arute, K. Arya, R. Babbush, D. Bacon, J. C. Bardin, R. Barends, R. Biswas, S. Boixo, F. G. S. L. Brandao, D. A. Buell, B. Burkett, Y. Chen, Z. Chen, B. Chiaro, R. Collins, W. Courtney, A. Dunsworth, E. Farhi, B. Foxen, A. Fowler, C. Gidney, M. Giustina, R. Graff, K. Guerin, S. Habegger, M. P. Harrigan, M. J. Hartmann, A. Ho, M. Hoffmann, T. Huang, T. S. Humble, S. V. Isakov, E. Jeffrey, Z. Jiang, D. Kafri, K. Kechedzhi, J. Kelly, P. V. Klimov, S. Knysh, A. Korotkov, F. Kostritsa, D. Landhuis, M. Lindmark, E. Lucero, D. Lyakh, S. Mandrà, J. R. McClean, M. McEwen, A. Megrant, X. Mi, K. Michelsen, M. Mohseni, J. Mutus, O. Naaman, M. Neeley, C. Neill, M. Y. Niu, E. Ostby, A. Petukhov, J. C. Platt, C. Quintana, E. G. Rieffel, P. Roushan, N. C. Rubin, D. Sank, K. J. Satzinger, V. Smelyanskiy, K. J. Sung, M. D. Trevithick, A. Vainsencher, B. Villalonga,

- T. White, Z. J. Yao, P. Yeh, A. Zalcman, H. Neven, and J. M. Martinis, *Quantum supremacy using a programmable superconducting processor*, Nature **574**, 505–510 (2019).
- [10] H.-S. Zhong, H. Wang, Y.-H. Deng, M.-C. Chen, L.-C. Peng, Y.-H. Luo, J. Qin, D. Wu, X. Ding, Y. Hu, P. Hu, X.-Y. Yang, W.-J. Zhang, H. Li, Y. Li, X. Jiang, L. Gan, G. Yang, L. You, Z. Wang, L. Li, N.-L. Liu, C.-Y. Lu, and J.-W. Pan, *Quantum computational advantage using photons*, Science **370**, 1460–1463 (2020).
- [11] J. Preskill, *Quantum Computing in the NISQ era and beyond*, Quantum **2**, 79 (2018).
- [12] A. Peruzzo, J. McClean, P. Shadbolt, M.-H. Yung, X.-Q. Zhou, P. J. Love, A. Aspuru-Guzik, and J. L. O’Brien, *A variational eigenvalue solver on a photonic quantum processor*, Nature Communications **5** (2014).
- [13] S. Sachdev, *Quantum Phase Transitions*, Cambridge University Press, 2 edition (2011).
- [14] V. S. Shchesnovich. *The second quantization method for indistinguishable particles (Lecture Notes in Physics, UFABC 2010)*, (2013).
- [15] F. T. Arecchi, E. Courtens, R. Gilmore, and H. Thomas, *Atomic Coherent States in Quantum Optics*, Phys. Rev. A **6**, 2211–2237 (1972).
- [16] N. N. Bogolyubov, *On the theory of superfluidity*, J. Phys. (USSR) **11**, 23–32 (1947).
- [17] M. P. A. Fisher, P. B. Weichman, G. Grinstein, and D. S. Fisher, *Boson localization and the superfluid-insulator transition*, Phys. Rev. B **40**, 546–570 (1989).
- [18] B. Capogrosso-Sansone, S. G. Soyler, N. Prokof’ev, and B. Svistunov, *Monte Carlo study of the two-dimensional Bose-Hubbard model*, Physical Review A **77**, 015602 (2008).
- [19] T. Dornheim, *Fermion sign problem in path integral Monte Carlo simulations: Quantum dots, ultracold atoms, and warm dense matter*, Physical Review E **100** (2019).
- [20] B. Capogrosso-Sansone, N. V. Prokof’ev, and B. V. Svistunov, *Phase diagram and thermodynamics of the three-dimensional Bose-Hubbard model*, Phys. Rev. B **75**, 134302 (2007).
- [21] J. K. Freericks and H. Monien, *Phase diagram of the Bose-Hubbard Model*, Euro-physics Letters (EPL) **26**, 545–550 (1994).
- [22] S. R. White, *Density matrix formulation for quantum renormalization groups*, Phys. Rev. Lett. **69**, 2863–2866 (1992).
- [23] Qiskit Textbook. *Quantum Phase Estimation*. <https://qiskit.org/textbook/ch-algorithms/quantum-phase-estimation.html>.

-
- [24] S. Gupta, S. Roy, B. Behera, and P. Panigrahi. *Quantum Simulation of One Dimensional Bose-Hubbard Model Using IBM Quantum Computer*, (2019).
- [25] Y. Yanay, J. Braumüller, S. Gustavsson, W. D. Oliver, and C. Tahan, *Two-dimensional hard-core Bose-Hubbard model with superconducting qubits*, npj Quantum Information **6** (2020).
- [26] M. Motta, C. Sun, A. T. K. Tan, M. J. O'Rourke, E. Ye, A. J. Minnich, F. G. S. L. Brandão, and G. K.-L. Chan, *Determining eigenstates and thermal states on a quantum computer using quantum imaginary time evolution*, Nature Physics **16**, 205–210 (2019).
- [27] S. Yalouz, B. Senjean, F. Miatto, and V. Dunjko. *Encoding strongly-correlated many-boson wavefunctions on a photonic quantum computer: application to the attractive Bose-Hubbard model*, (2021).
- [28] K. Kottmann, F. Metz, J. Fraxanet, and N. Baldelli. *Variational Quantum Anomaly Detection: Unsupervised mapping of phase diagrams on a physical quantum computer*, (2021).
- [29] M. Łącki, B. Damski, and J. Zakrzewski. *Locating the quantum critical point of the Bose-Hubbard model through singularities of simple observables*, (2016).
- [30] I. Danshita and A. Polkovnikov, *Superfluid-to-Mott-insulator transition in the one-dimensional Bose-Hubbard model for arbitrary integer filling factors*, Physical Review A **84** (2011).
- [31] M. Galante, G. Mazzarella, and L. Salasnich. *Analytical results on quantum correlations of few bosons in a double-well trap*, (2014).
- [32] Y. P. Huang and M. G. Moore, *Creation, detection, and decoherence of macroscopic quantum superposition states in double-well Bose-Einstein condensates*, Phys. Rev. A **73**, 023606 (2006).
- [33] I. Frerot and T. Roscilde, *Entanglement Entropy across the Superfluid-Insulator Transition: A Signature of Bosonic Criticality*, Physical Review Letters **116** (2016).
- [34] S. Subramanian and M.-H. Hsieh, *Quantum algorithm for estimating alpha-Renyi entropies of quantum states*, Physical Review A **104** (2021).
- [35] M. A. Nielsen, *Cluster-state quantum computation*, Reports on Mathematical Physics **57**, 147–161 (2006).
- [36] M. A. Nielsen and I. L. Chuang, *Quantum Computation and Quantum Information: 10th Anniversary Edition*, Cambridge University Press, USA, 10th edition (2011).
- [37] C. Moran, *Mastering Quantum Computing with IBM QX: Explore the World of Quantum Computing Using the Quantum Composer and Qiskit*, Packt Publishing (2019).

- [38] N. Moll, P. Barkoutsos, L. S. Bishop, J. M. Chow, A. Cross, D. J. Egger, S. Filipp, A. Fuhrer, J. M. Gambetta, M. Ganzhorn, A. Kandala, A. Mezzacapo, P. Müller, W. Riess, G. Salis, J. Smolin, I. Tavernelli, and K. Temme, *Quantum optimization using variational algorithms on near-term quantum devices*, Quantum Science and Technology **3**, 030503 (2018).
- [39] A. W. Cross, L. S. Bishop, S. Sheldon, P. D. Nation, and J. M. Gambetta, *Validating quantum computers using randomized model circuits*, Physical Review A **100** (2019).
- [40] M. G. A. Paris, *The modern tools of quantum mechanics*, The European Physical Journal Special Topics **203**, 61–86 (2012).
- [41] M. S. Jattana, F. Jin, H. De Raedt, and K. Michielsen, *General error mitigation for quantum circuits*, Quantum Information Processing **19**, 414 (2020).
- [42] M. Cerezo, A. Arrasmith, R. Babbush, S. C. Benjamin, S. Endo, K. Fujii, J. R. McClean, K. Mitarai, X. Yuan, L. Cincio, and P. J. Coles, *Variational quantum algorithms*, Nature Reviews Physics **3**, 625–644 (2021).
- [43] P. K. Barkoutsos, J. F. Gonthier, I. Sokolov, N. Moll, G. Salis, A. Fuhrer, M. Ganzhorn, D. J. Egger, M. Troyer, A. Mezzacapo, S. Filipp, and I. Tavernelli, *Quantum algorithms for electronic structure calculations: Particle-hole Hamiltonian and optimized wave-function expansions*, Phys. Rev. A **98**, 022322 (2018).
- [44] G. Salis and N. Moll. *Short-depth trial-wavefunctions for the variational quantum eigensolver based on the problem Hamiltonian*, (2019).
- [45] A. Kandala, A. Mezzacapo, K. Temme, M. Takita, M. Brink, J. M. Chow, and J. M. Gambetta, *Hardware-efficient variational quantum eigensolver for small molecules and quantum magnets*, Nature **549**, 242–246 (2017).
- [46] S. Barison, D. E. Galli, and M. Motta. *Quantum simulations of molecular systems with intrinsic atomic orbitals*, (2020).
- [47] S. B. Bravyi and A. Y. Kitaev, *Fermionic Quantum Computation*, Annals of Physics **298**, 210–226 (2002).
- [48] G. Ortiz, J. E. Gubernatis, E. Knill, and R. Laflamme, *Quantum algorithms for fermionic simulations*, Phys. Rev. A **64**, 022319 (2001).
- [49] C. D. Batista and G. Ortiz, *Algebraic approach to interacting quantum systems*, Advances in Physics **53**, 1–82 (2004).
- [50] Y. Tong, V. V. Albert, J. R. McClean, J. Preskill, and Y. Su. *Provably accurate simulation of gauge theories and bosonic systems*, (2021).
- [51] L.-A. Wu and D. A. Lidar, *Qubits as parafermions*, Journal of Mathematical Physics **43**, 4506–4525 (2002).

-
- [52] R. D. Somma, G. Ortiz, E. H. Knill, and J. Gubernatis, *Quantum simulations of physics problems*, Quantum Information and Computation **5***105* (2003).
 - [53] N. P. D. Sawaya, T. Menke, T. H. Kyaw, S. Johri, A. Aspuru-Guzik, and G. G. Guerreschi, *Resource-efficient digital quantum simulation of d-level systems for photonic, vibrational, and spin-s Hamiltonians*, npj Quantum Information **6** (2020).
 - [54] IBM Quantum. *Learn quantum computing, a field guide: Entanglement*. <https://quantum-computing.ibm.com/composer/docs/iqx/guide/entanglement>.
 - [55] K. Setia, R. Chen, J. E. Rice, A. Mezzacapo, M. Pistoia, and J. D. Whitfield, *Reducing Qubit Requirements for Quantum Simulations Using Molecular Point Group Symmetries*, Journal of Chemical Theory and Computation **16**, 6091–6097 (2020).
 - [56] W.-B. Gao, C.-Y. Lu, X.-C. Yao, P. Xu, O. Gühne, A. Goebel, Y.-A. Chen, C.-Z. Peng, Z.-B. Chen, and J.-W. Pan, *Experimental demonstration of a hyper-entangled ten-qubit Schrödinger cat state*, Nature Physics **6**, 331–335 (2010).
 - [57] I. G. Ryabinkin, S. N. Genin, and A. F. Izmaylov. *Constrained variational quantum eigensolver: Quantum computer search engine in the Fock space*, (2018).
 - [58] M. Sarovar, T. Proctor, K. Rudinger, K. Young, E. Nielsen, and R. Blume-Kohout, *Detecting crosstalk errors in quantum information processors*, Quantum **4**, 321 (2020).